Current Chemistry Letters 14 (2025) 79–106

Contents lists available at GrowingScience

Current Chemistry Letters

homepage: www.GrowingScience.com

Integrated computer aided methods to designing potent α-Glucosidase inhibitors based on quinoline scaffold derivatives

Ayoub Khaldan[a*], Soukaina Bouamrane[a], Reda El-Mernissi[a], Marwa Alaqarbeh[b], Hamid Maghat[a], Mohammed Bouachrine[a,c], Tahar Lakhlifi[a] and Abdelouahid Sbai[a]

[a]*Molecular Chemistry and Natural Substances Laboratory, Faculty of Science, Moulay Ismail University of Meknes, Morocco*
[b]*Basic Science Department, Prince Al Hussein Bin Abdullah II Academy for Civil Protection, Al-Balqa Applied University, Al-Salt 19117, Jordan*
[c]*EST Khenifra, Sultan Moulay Sliman University, Benimellal, Morocco*

C H R O N I C L E

Article history:
Received July 20, 2024
Received in revised form
August 3, 2024
Accepted September 1, 2024
Available online
September 7, 2024

Keywords:
α-Glucosidase
Molecular Modelling
MD simulations
ADME/Tox
DFT

A B S T R A C T

Diabetes mellitus is a serious health disease that affects people all over the world. The number of persons identified with diabetes mellitus rises each year. α -Glucosidase is a digestive enzyme used to control diabetes mellitus. The searching for new potent α-glucosidase inhibitors capable of delaying carbohydrate digestion in the human body is an important strategy towards control of diabetes mellitus. In this work, a series of quinoline-based Schiff base derivatives already identified as α-glucosidase inhibitory activity was studied by using 2D/3D-QSAR approach. The best HQSAR/A-B-C-H-Ch-DA and CoMSIA/SEDA models were constructed using thirteen molecules in the training set, resulting in favorable values of Q2 (0.834 and 0.607), and high values of R2 (0.985 and 0.912), respectively. The generated HQSAR/A-B-C-H-Ch-DA and CoMSIA/SEDA contour plots were precious for designing and enhancing the α-glucosidase inhibitory activity of quinoline-based Schiff base molecules. Considering these results, two novel α-glucosidase compounds were designed to possess significant activity. The newly suggested molecules showed good outcomes in the preliminary in silico ADME/Tox evaluations. Molecular docking results revealed that the new designed inhibitors have a good stability in the active pocket of the studied receptor compared to voglibose, clinically used as an α-glucosidase inhibitor. MD simulation and MM-GBSA results confirmed the molecular docking outcomes. Finally, DFT analysis was useful in determining the most electrophilic and nucleophilic centers of the two designed α-glucosidase inhibitors.

1. Introduction

Diabetes mellitus is a metabolic condition identified by elevated glucose levels in the bloodstream. The main concern is postprandial hyperglycemia, where blood sugar rises after meals due to insufficient insulin action or production, leading to potential complications if not properly managed.[1,2] Diabetes frequently presents with ketosis and the loss of protein [3], in addition to various other complications like neuropathy, retinopathy, and peripheral vascular deficiencies.[4] Diabetes is one of the most severe health problems of the present era, which is impacting millions of people throughout the world, particularly in developing countries.[5] According to the International Diabetes Federation, the number of people with diabetes exceeded 366 million in 2011 and is projected to rise significantly to reach 552 million by the year 2030.[6,7] Type 2 diabetes mellitus is more commonly found in developed nations and is distinguished by decreased sensitivity to insulin and impaired insulin secretion.[8,9] α-Glucosidase is a digestive enzyme located in the epithelium cell lining of the small

* Corresponding author
E-mail address a.khaldan@edu.umi.ac.ma (A. Khaldan)

doi: 10.5267/j.ccl.2024.9.003

intestine.[10] The enzyme breaks disaccharides and polysaccharides into glucose.[11] α-Glucosidase inhibition is a vital strategy in managing blood glucose levels, particularly in individuals with diabetes. By slowing down the action of α-glucosidase, this inhibition reduces the rapid breakdown of complex carbohydrates into glucose, leading to a more gradual release of sugar into the bloodstream after meals. This controlled glucose absorption helps maintain normal blood glucose levels, minimizing the risk of postprandial hyperglycemia and its associated complications.[12] Acarbose [13], voglibose and miglitol [14] are α-glucosidase inhibitors used extensively in the clinic to treat diabetes mellitus. However, continuous administration of these medications may cause several unwanted effects such as diarrhea and abdominal discomfort.[15,16] As a result, there is an urgent requirement for novel α-glucosidase medications that exhibit improved efficacy in controlling postprandial hyperglycemia while causing fewer unwanted side effects.

Quinolines and their derivatives play a role in regulating diabetic conditions by exhibiting hypoglycemic activity, influencing glucidic metabolism. Additionally, quinolines possess various other biological activities, such as antimalarial,[17] anticancer,[18] and anti-inflammatory effects.[19] Some studies suggest that quinolines might indirectly induce hypoglycemia through mechanisms resembling those of sulfonylureas.[20] The three-dimensional quantitative structure-activity relationship (3D-QSAR) model is a powerful computational tool that analyzes the relationship between the three-dimensional structure of molecules and their biological activity.[21-25] Its widespread application spans diverse scientific disciplines, including drug design, environmental risk assessment, and chemical safety evaluation.[26-28] In molecular toxicity detection, the 3D-QSAR model helps identify potential hazards and assess the safety of chemical compounds, while in biological activity prediction, it aids in understanding the interactions between molecules and their target receptors, enabling the discovery of new therapeutic agents.[29,30] One of the widely used techniques in QSAR is comparative molecular similarity indexes analysis (CoMSIA),[31] which correlates alterations in the 3D structural features of chemical moieties, such as steric, electrostatic, and hydrophobic properties, with their biological activity. CoMSIA is valuable in understanding how these structural factors influence the interaction between molecules and their target receptors, providing valuable insights for drug design and optimization processes.[32] Molecular docking simulation has emerged as a fundamental and essential approach in the field of molecular modeling.[33] It plays a central role in predicting and analyzing the interactions between small molecules, such as drugs or ligands, and their target proteins or biomolecules. Molecular docking simulations provide valuable insights into the binding modes, affinities, and molecular interactions, aiding in drug discovery, protein-ligand interaction studies, and the design of novel therapeutics.[34]

The objective of this research was to explore the Structure-Activity Relationship (SAR) of a specific set of quinoline-based Schiff base molecules to determine the key structural features that influence their activity. By understanding these relationships, the study aims to propose novel inhibitors for α-glucosidase with enhanced and promising activity, potentially contributing to the development of diabetes management medications that are both more efficient and safer.

2. Results and Discussion

2.1 HQSAR Result

The HQSAR is a QSAR analysis approach that offers several advantages over traditional methods. One of the key benefits of HQSAR is that it eliminates the need for molecular alignment, the creation of 3D structures, and the consideration of potential binding conformations, making the process more efficient and less computationally intensive. HQSAR allows for the examination of the relationship between each compound studied and its biological activity. It achieves this by encoding the molecular structure of each compound into a hologram, which represents a simplified, yet informative, representation of the molecule's features. The effectiveness of the HQSAR model is influenced by three main factors: fragment type (fragment distinction), hologram length, and fragment size. The statistical metrics for the HQSAR models are listed in **Table 1.** A total of 54 HQSAR models were created by combining different fragment distinctions. Among these models, the one ranked as the best is labeled as N° 54. For this model, the fragments making up the selected model are atoms (A), bonds (B), connections (C), hydrogen atoms (H), chirality (Ch), donor and acceptor (DA). To determine the optimal fragment size, a range from 3-6 to 16-19 was tested, and the best size was selected based on the model's performance. **Table 2** presents the statistical results of the HQSAR model with the combination of A/B/C/H/Ch/DA fragments, which was identified as the most promising model in the investigation. The HQSAR/A-B-C-H-Ch-DA model has a Q^2 value of 0.834, a standard error of 0.147, R^2 value of 0.985, EES of 0.045, using an acceptable hologram length (HL) of 61, and fragment size of 4-7. The statistical results obtained demonstrated the robustness and effectiveness of the HQSAR/A-B-C-H-Ch-DA model.

Table 3 provides the actual and estimated α-glucosidase inhibitor activities for the investigated molecules. **Fig. 1** displays graphs illustrating the experimental and estimated α-glucosidase activity values for all the compounds used in developing the HQSAR/A-B-C-H-Ch-DA model. In the graphs, the training set molecules are depicted as blue squares, and the test set compounds are shown as red triangles. The solid points of these blue squares and red triangles are tightly grouped around the Y = X line, demonstrating a robust linear relationship between the observed and predicted α-glucosidase inhibitory activity of the inhibitors under study.

Table 1. HQSAR results for various fragment distinctions based on fragment sizes ranging from 4 to 7.

Model no.	Fragment distinction	N	$Q^{2\,a}$	$Std\ Error^{b}$	$R^{2\,c}$	SEE^{d}	BHL^{e}
1	A	6	0.693	0.216	0.997	0.020	257
2	C	2	0.617	0.187	0.799	0.135	151
3	DA	3	0.731	0.165	0.918	0.091	61
4	A/B	6	0.706	0.211	0.998	0.017	257
5	A/C	6	0.629	0.237	0.998	0.019	401
6	A/H	6	0.677	0.221	0.997	0.020	83
7	A/Ch	6	0.646	0.232	0.997	0.021	257
8	A/D	3	0.731	0.165	0.918	0.091	61
9	B/C	6	0.731	0.202	0.989	0.042	97
10	B/DA	4	0.772	0.161	0.980	0.048	83
11	C/H	2	0.617	0.187	0.799	0.135	151
12	C/Ch	2	0.617	0.187	0.799	0.135	151
13	C/DA	3	0.744	0.161	0.921	0.089	151
14	H/DA	3	0.764	0.154	0.915	0.093	61
15	Ch/DA	3	0.764	0.151	0.915	0.093	61
16	A/B/C	6	0.642	0.233	0.994	0.030	353
17	A/B/H	6	0.793	0.177	0.994	0.031	61
18	A/B/Ch	6	0.697	0.215	0.998	0.018	257
19	A/B/DA	5	0.776	0.171	0.990	0.036	83
20	A/C/H	5	0.586	0.232	0.994	0.027	71
21	A/C/Ch	6	0.629	0.237	0.998	0.019	401
22	A/C/DA	3	0.774	0.151	0.953	0.069	401
23	A/H/Ch	3	0.731	0.202	0.999	0.009	53
24	A/H/DA	4	0.752	0.168	0.965	0.063	53
25	B/C/H	6	0.731	0.202	0.989	0.042	97
26	B/C/Ch	6	0.731	0.202	0.989	0.042	97
27	B/C/DA	6	0.789	0.179	0.994	0.031	401
28	B/H/DA	4	0.772	0.161	0.980	0.048	83
29	B/Ch/DA	4	0.772	0.161	0.980	0.048	83
30	C/H/Ch	2	0.617	0.187	0.799	0.135	151
31	C/H/DA	3	0.744	0.161	0.921	0.089	151
32	H/Ch/DA	3	0.764	0.154	0.915	0.093	61
33	A/B/C/H	4	0.776	0.160	0.981	0.046	97
34	A/B/C/Ch	6	0.642	0.233	0.994	0.030	353
35	A/B/C/DA	3	0.794	0.144	0.931	0.084	199
36	A/B/H/Ch	6	0.746	0.196	0.997	0.022	61
37	A/B/H/DA	4	0.786	0.156	0.954	0.072	97
38	A/B/Ch/DA	3	0.708	0.172	0.908	0.096	59
39	A/B/C/H/DA	6	0.766	0.188	0.988	0.043	97
40	A/C/H/Ch	5	0.586	0.232	0.994	0.027	71
41	A/C/H/DA	4	0.706	0.183	0.946	0.078	83
42	B/C/H/Ch	6	0.731	0.202	0.989	0.042	97
43	B/C/H/DA	6	0.789	0.179	0.994	0.031	401
44	C/H/Ch/DA	3	0.744	0.161	0.921	0.089	151
45	B/H/Ch/DA	4	0.772	0.161	0.980	0.048	83
46	B/C/Ch/DA	6	0.789	0.179	0.994	0.031	401
47	A/B/C/H/Ch	4	0.776	0.160	0.981	0.046	97
48	A/B/C/H/DA	6	0.766	0.188	0.988	0.043	97
49	A/B/C/Ch/DA	5	0.782	0.168	0.981	0.049	353
50	A/B/H/Ch/DA	4	0.762	0.165	0.955	0.071	97
51	A/C/H/Ch/DA	4	0.731	0.175	0.965	0.063	307
52	B/C/H/Ch/DA	6	0.789	0.179	0.994	0.031	401
53	A/B/C/Ch/DA	5	0.782	0.168	0.981	0.049	353
54	**A/B/C/H/Ch/DA**	**5**	**0.834**	**0.147**	**0.985**	**0.045**	**61**

R^2: non-cross-validated correlation coefficient; Q2: cross-validated correlation coefficient; Std Error: standard error; N: optimal number of components; SEE: standard estimated error; BHL: best hologram length. The optimal model is highlighted in bold.

Table 2. Statistical outcomes of model No. 54 with different fragment sizes.

Model no.	Fragment	N	$Q^{2\,a}$	Std Error^{b}	$R^{2\,c}$	SEE^{d}	BHL^{e}
3-6	A/B/C/H/Ch/DA	4	0.780	0.158	0.944	0.080	61
4-7	**A/B/C/H/Ch/DA**	**5**	**0.834**	**0.147**	**0.985**	**0.045**	**61**
5-8	A/B/C/H/Ch/DA	4	0.746	0.170	0.978	0.050	61
6-9	A/B/C/H/Ch/DA	6	0.564	0.257	0.997	0.022	61
7-10	A/B/C/H/Ch/DA	3	0.576	0.207	0.937	0.080	61
8-11	A/B/C/H/Ch/DA	3	0.608	0.199	0.958	0.064	61
9-12	A/B/C/H/Ch/DA	5	0.642	0.216	0.997	0.021	61
10-13	A/B/C/H/Ch/DA	1	0.475	0.209	0.601	0.209	61
11-14	A/B/C/H/Ch/DA	1	0.448	0.214	0.578	0.187	61
12-15	A/B/C/H/Ch/DA	3	0.532	0.203	0.691	0.204	61
13-16	A/B/C/H/Ch/DA	2	0.631	0.163	0.771	0.096	61
14-17	A/B/C/H/Ch/DA	3	0.552	0.215	0.710	0.163	61
15-18	A/B/C/H/Ch/DA	2	0.612	0.152	0.747	0.075	61
16-19	A/B/C/H/Ch/DA	2	0.625	0.118	0.758	0.126	61

Table 3. Observed and predicted pIC_{50} activity of the investigated molecules using HQSAR/A-B-C-H-Ch-DA model.

N°	pIC_{50} (Obs)	HQSAR/A-B-C-H-Ch-DA		N°	pIC_{50} (Obs)	HQSAR/A-B-C-H-Ch-DA		N°	pIC_{50} (Obs)	HQSAR/A-B-C-H-Ch-DA	
		pIC_{50} (Pred)	Residuals			pIC_{50} (Pred)	Residuals			pIC_{50} (Pred)	Residuals
1	4.907	4.879	0.028	**7**[a]	4.666	4.559	0.107	**13**	4.629	4.669	-0.040
2	5.027	5.013	0.014	**8**	4.842	4.851	-0.009	**14**	4.879	4.863	0.016
3	4.851	4.839	0.012	**9**[a]	5.131	5.112	0.019	**15**	4.447	4.465	-0.018
4	5.208	5.237	-0.029	**10**	4.317	4.374	-0.057	**16**	4.544	4.544	0.000
5[a]	4.425	4.362	0.063	**11**	4.539	4.462	0.077	**17**	4.415	4.395	0.020
6[a]	4.735	4.532	0.203	**12**	4.416	4.428	-0.012	[a] *Test set molecules*			

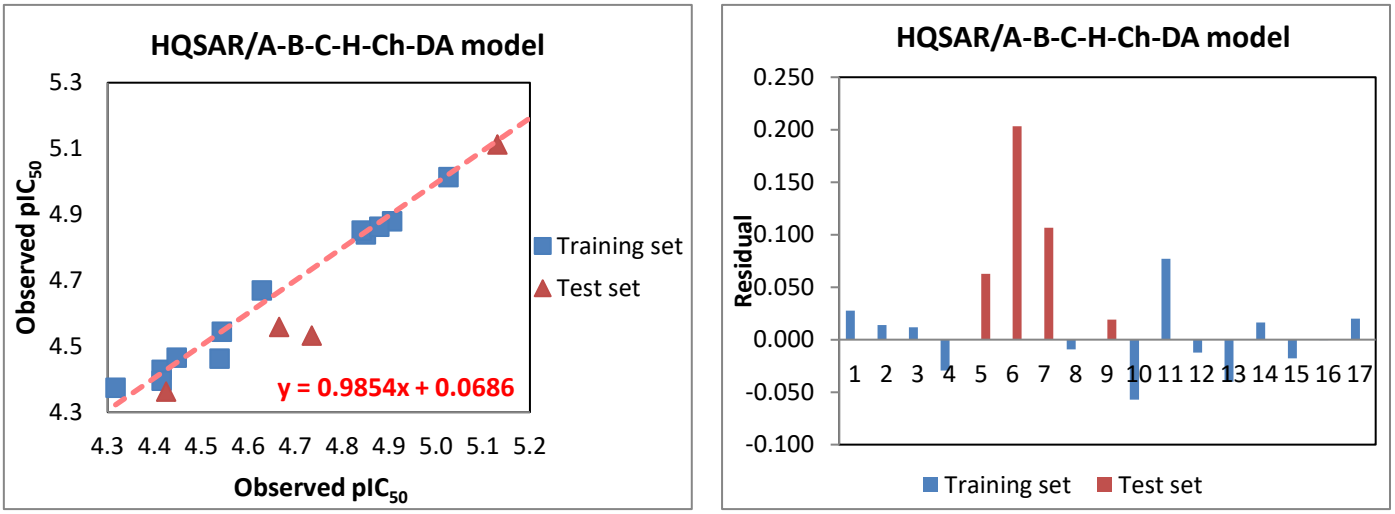

Fig. 1. Plots of predicted versus observed pIC_{50} values for the investigated molecules, along with their residuals, using the HQSAR/A-B-C-H-Ch-DA model.

2.2 Statistical CoMSIA Results

A cross-validated Q^2 value greater than 0.5 indicates acceptable internal predictive capability and the strength of the model but it is not an absolute proof of the model's accuracy. Cross-validation helps assess how well the model performs on the data used for training, but it does not guarantee the model's ability to generalize to new, unseen data. External validation, on the other hand, is a crucial step in evaluating the predictive power of a model. It involves testing the model on a separate set of molecules (test set) that were not used during the model's training process. The metric commonly used for external validation is the R^2pred. Indeed, R^2pred value greater than 0.6 is generally considered as an acceptable level of predictive power for the model.

In this section of the study, various CoMSIA models have been constructed, and the statistical outcomes of these models, obtained through PLS analysis, are presented in **Table 4**. Considering the statistical significance of the data, it was observed that the CoMSIA/SEDA model outperformed all other CoMSIA models that were proposed in the study. Indeed, CoMSIA/SEDA model exhibits impressive statistical metrics, with a Q^2 value of 0.607, R^2 value of 0.912, and F value of 31.131 as well as SEE of 0.094. Continuously, the CoMSIA model underwent external validation to assess its predictive capability, and the obtained R^2pred was 0.85. This value surpasses the threshold of 0.6, indicating that the CoMSIA/SEDA model possesses strong predictive power. Furthermore, the findings from **Table 4** indicate that the developed CoMSIA/SEDA model comprises four fields, with the acceptor and donor fields being the most influential in determining the molecular properties or activities under investigation.

The real and estimated α-glucosidase inhibitors activities of the 17 quinoline-based Schiff base molecules are given in **Table 5**. As evident from the data presented in **Table 5**, the residuals between the actual and predicted α-glucosidase inhibitor activities of the investigated molecules are very small, all being less than 1. This result serves as strong evidence of the model's efficacy and its ability to reliably predict the α-glucosidase inhibitory activity of new molecules.
Fig. 2 shows the graphs illustrating the observed versus predicted α-glucosidase activity values for all the molecules used in developing the CoMSIA/SEDA model. In these graphs, the training set molecules are depicted as blue circles, and the test set compounds are represented by red triangles. The graphs demonstrate a strong linear correlation between the observed and predicted α-glucosidase inhibitory activity of the studied inhibitors.

Table 4. Different developed CoMSIA models with statistical results.

Model	Q^2	R^2	SEE	F	N	R^2pred	Fractions				
							Ster	Elec	Acc	Don	Hyd
CoMSIA/SEA	0.636	0.952	0.074	40.076	4	0.60	0.092	0.117	0.791	-	-
CoMSIA/SHA	0.490	0.957	0.070	44.948	4	0.61	0.066	-	0.768	-	0.166
CoMSIA/SDA	0.60	0.941	0.077	48.126	3	0.74	0.044	-	0.412	0.544	-
CoMSIA/EHD	0.520	0.879	0.111	21.716	3	0.01	-	0.100	-	0.760	0.140
CoMSIA/EDA	0.560	0.81	0.131	21.479	2	0.77	-	0.121	0.300	0.579	-
CoMSIA/HDA	0.570	0.892	0.099	41.414	2	0.76	-		0.382	0.504	0.114
CoMSIA/EHDA	0.563	0.909	0.096	30.088	3	0.77	-	0.073	0.344	0.491	0.092
CoMSIA/SHDA	0.557	0.890	0.100	40.470	2	0.74	0.038	-	0.365	0.490	0.107
CoMSIA/SEDA	**0.607**	**0.912**	**0.094**	**31.181**	**3**	**0.90**	**0.039**	**0.085**	**0.361**	**0.516**	**-**
CoMSIA/SEHA	0.480	0.953	0.073	40.797	4	0.63	0.063	0.094	0.699	-	0.145
CoMSIA/SEHD	0.518	0.876	0.112	21.136	3	0.55	0.050	0.095	-	0.725	0.130
CoMSIA/SEHDA	0.561	0.906	0.097	29.047	3	0.75	0.034	0.071	0.331	0.477	0.087

R^2: Non-cross-validated correlation coefficient, F: F-test value, SEE: Standard error of the estimate, Q^2: Cross-validated correlation coefficient, N: Optimum number of components, R^2pred: External validation correlation coefficient.

Table 5. Observed and predicted pIC_{50} activity of the investigated molecules using CoMSIA/SEDA model

N°	pIC_{50} (Obs)	CoMSIA/SEDA		N°	pIC_{50} (Obs)	CoMSIA/SEDA		N°	pIC_{50} (Obs)	CoMSIA/SEDA	
		pIC_{50} (Pred)	Residuals			pIC_{50} (Pred)	Residuals			pIC_{50} (Pred)	Residuals
1	4.907	4.782	0.125	**7**[a]	4.666	4.751	-0.085	**13**	4.629	4.696	-0.067
2	5.027	5.060	-0.033	**8**	4.842	4.868	-0.026	**14**	4.879	4.813	0.066
3	4.851	4.938	-0.087	**9**[a]	5.131	5.039	0.092	**15**	4.447	4.566	-0.119
4	5.208	5.154	0.054	**10**	4.317	4.432	-0.115	**16**	4.544	4.435	0.109
5[a]	4.425	4.365	0.060	**11**	4.539	4.446	0.093	**17**	4.415	4.422	-0.007
6[a]	4.735	4.801	-0.066	**12**	4.416	4.411	0.005	[a] *Test set molecules*			

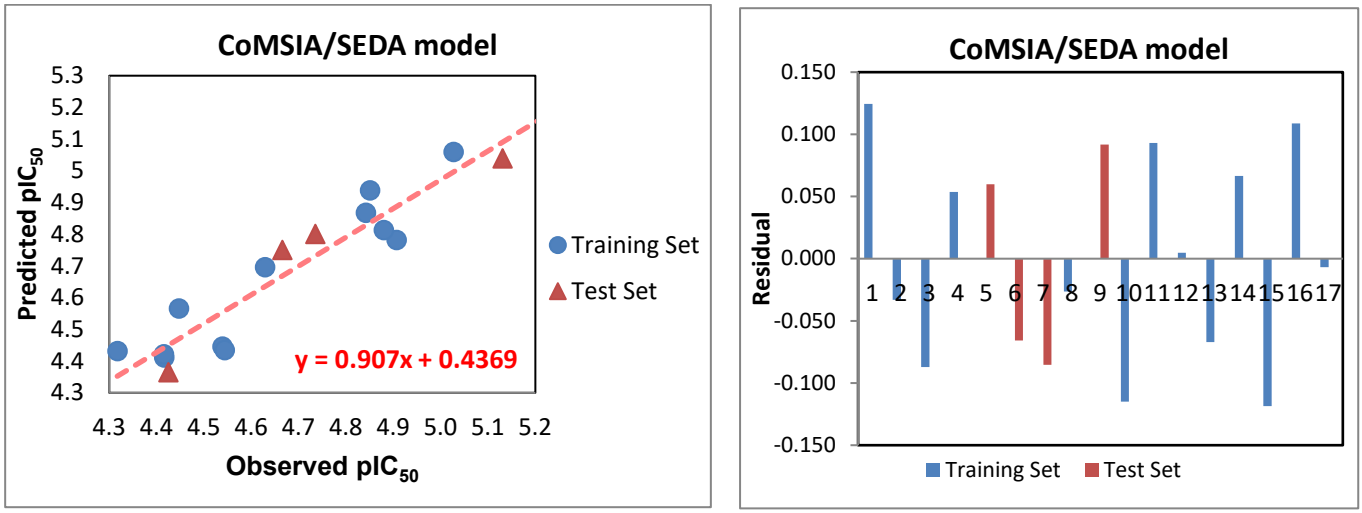

Fig. 2. Plots of predicted versus observed pIC_{50} values for the investigated molecules, along with their residuals, using the CoMSIA/ SEDA model.

2.3 Validation of 2D/3D-QSAR Models

The predictive capabilities of both the HQSAR/A-B-C-H-Ch-DA and CoMSIA/SEDA models were thoroughly assessed through external validation, employing the Golbraikh and Tropsha criteria, as well as the Roy criterion. To conduct this evaluation, four test molecules based on quinoline-based Schiff bases were utilized. The findings from the external validation of the 2D/3D-QSAR model are listed in **Table 6**.

According to the data presented in **Table 6**, both the HQSAR/A-B-C-H-Ch-DA and CoMSIA/SEDA models demonstrate reliable results within the Golbraikh and Tropsha parameters, indicating that they meet the specified criteria. Additionally, the values of r_m^2 and $r_m'^2$ for the HQSAR/A-B-C-H-Ch-DA and CoMSIA/SEDA models are 0.71 and 0.63, and 0.65 and 0.63, respectively, all of which exceed the threshold of 0.5. Moreover, the models exhibit a Δr_m^2 value below 0.2 and a Δr_0^2 value not exceeding 0.3. As a result, both the HQSAR/A-B-C-H-Ch-DA and CoMSIA/SEDA models have successfully met the requirements of the Roy criterion.

The HQSAR/A-B-C-H-Ch-DA and CoMSIA/SEDA models, which were selected as the preferred models, demonstrated high reliability and stability during the external validation tests. As a result, there is a high level of confidence in their aptitude to correctly predict the α-glucosidase activity of potential new molecules.

Table 6. External validation results of the HQSAR/A-B-C-H-Ch-DA and CoMSIA/SEDA models using Golbraikh, Tropsha, and Roy criteria.

Criteria	Parameter	Validation Criteria	HQSAR/A-B-C-H-Ch-DA	CoMSIA/SEDA
Golbraikh and Tropsha	r_0^2	$r_0^2 > 0.5$	0.885	0.99
	$r_0'^2$	$r_0'^2 > 0.5$	0.855	0.99
	r^2pred	$r^2 > 0.6$	0.94	0.90
	k	$0.85 \leq k \leq 1.15$	1.02	1.00
	$\frac{r^2 - r_0^2}{r^2}$	< 0.1	0.06	-0.101
	k'	$0.85 \leq k \leq 1.15$	0.97	0.999
	$\frac{r^2 - r_0'^2}{r^2}$	< 0.1	0.09	-0.101
Roy	r_m^2	$r_m^2 > 0.5$	0.71	0.63
	$r_m'^2$	$r_m'^2 > 0.5$	0.65	0.63
	Δr_m^2	$\Delta r_m^2 < 0.2$	-0.05	5.05×10^{-5}
	Δr_0^2	$\Delta r_0^2 < 0.3$	0.06	0.000

2.4 HQSAR Contribution Map

The HQSAR output computations are based on analyzing the individual molecular fragments within a molecule and their respective contributions to its α-glucosidase activity. The HQSAR findings analysis can be visually presented through a contribution map, which is represented as a color-coded structural diagram. In this diagram, each atom is assigned a specific color that corresponds to its contribution to the overall α-glucosidase activity of the compound. This graphical representation allows us to identify and understand the key structural elements that play a crucial role in the compound's α-glucosidase activities. In **Fig. 3**, the HQSAR contribution maps for two compounds, **C4** and **C10**, are presented. **C4** is the most active inhibitor in the dataset, while compound **C10** is the least active. The contribution maps use color coding to illustrate the impact of each atom on the compounds' overall α-glucosidase activity. Atoms contributing positively to the activity are represented by the colors green, blue, green-blue, and yellow. On the other hand, atoms contributing negatively to the activity are shown in red, red-orange, and orange. Contributions that fall in between positive and negative effects are depicted in white. In **Fig. 3 (a)**, the structural diagram of the **C4** molecule shows a quinoline fragment highlighted in a certain position in green color. This suggests that the quinoline moiety could have a crucial role in boosting the α-glucosidase inhibitory activity of the compound. On the contrary, **Fig. 3 (b)** shows the structural diagram of the **C10** molecule, where the green color is absent in the quinoline region. This absence of green color in the quinoline moiety could explain the lower activity of the **C10** molecule in the database. The HQSAR model is effective in explaining and reflecting the influence of specific fragments on α-glucosidase activity, as evidenced by the color-coded contribution maps for certain molecules. However, it has limitations in explaining and characterizing the contribution of other fragments that are represented as white in both molecules. As a result, the information provided by the three-dimensional CoMSIA approach proves to be more valuable in identifying favorable and unfavorable groups for α-glucosidase activity. These three-dimensional approaches offer deeper insights into the spatial interactions and steric effects of different molecular groups, enabling a more comprehensive understanding of their impact on α-glucosidase activity, which goes beyond what the HQSAR model can provide.

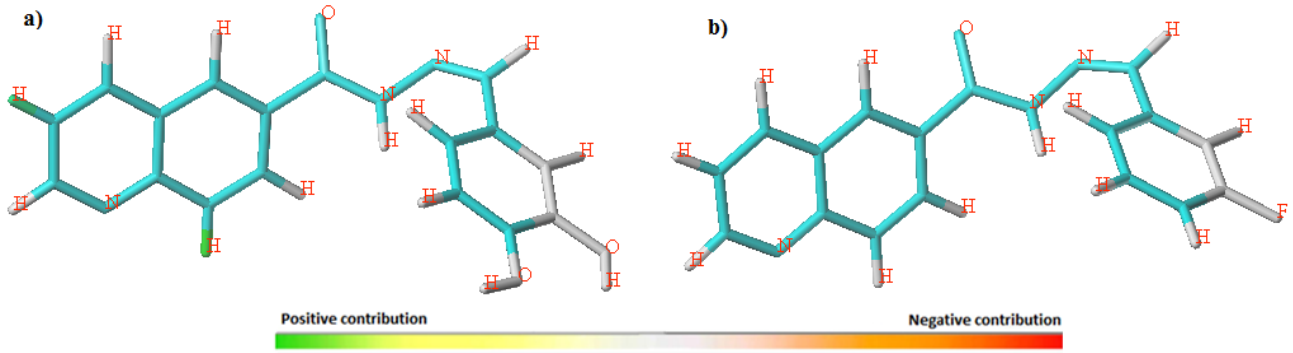

Fig. 3. HQSAR contribution map of molecules **C4** (a) and **C10** (b).

2.5 CoMSIA Contour Map

The contour maps generated from CoMSIA/SEDA model considered as important tools to clear up the significant structural aspects of compounds for the α-glucosidase inhibitory activity based on preferred and unpreferred sites of different fields. Therefore, suggesting new α-glucosidase inhibitors. **Fig. 4** elucidates the contour maps extracted from CoMSIA/SEDA model using the molecule **C4** as a template because it is the dataset's more active molecule.

CoMSIA steric contour map is revealed in **Fig. 4(a)**; where steric field embodied by yellow color with 20 % contribution, and green color with 80 % contribution. The portion that appears in green around *ortho* and *meta* positions of the R moiety illustrated that bulky entities at these sites ameliorated the α-glucosidase inhibitory activity. This can be easily known by comparing the structure of molecule **C2** (pIC_{50}=5.027) and compound **C13** (pIC_{50}= 4.629). Molecule **C2** consists two hydroxyl groups at *ortho* and *meta* positions of the R group while molecule **C13** possesses two hydrogen atoms. The yellow color around *ortho*, *meta* and *para* sites of the R moiety elucidated that small groups in these positions improved the biological activity. We can explain that by viewing the structure of molecule **C2** (pIC_{50}=5.027) and molecule **C13** (pIC_{50}= 4.629).

The R group's *ortho* position which is covered by blue and red colors demonstrates that this region can be occupied by both electro-donating and electro-withdrawing groups. On the other hand, the *meta* position of R group suggests that substituents with electron-donating behavior are favorable for α-glucosidase activity (**Fig. 4(b)**).

The magenta color located at *meta* position of phenyl moiety points out that groups with hydrogen bond acceptor behavior can ameliorate the inhibitory activity. The red color around *ortho* place of the R group and 2-methylenehydrazine moiety indicates that groups with hydrogen bond donor behavior are required in these positions to enhance the activity (**Fig. 4(c)**).

Fig. 4(d) indicates that entities with hydrogen bond donor behavior at ortho and *meta* positions of phenyl entity could ameliorate the activity of molecules. **Fig. 4(d)** also shows also that moiety with hydrogen bond donor behavior in all positions of R group might improve the α-glucosidase inhibitory activity.

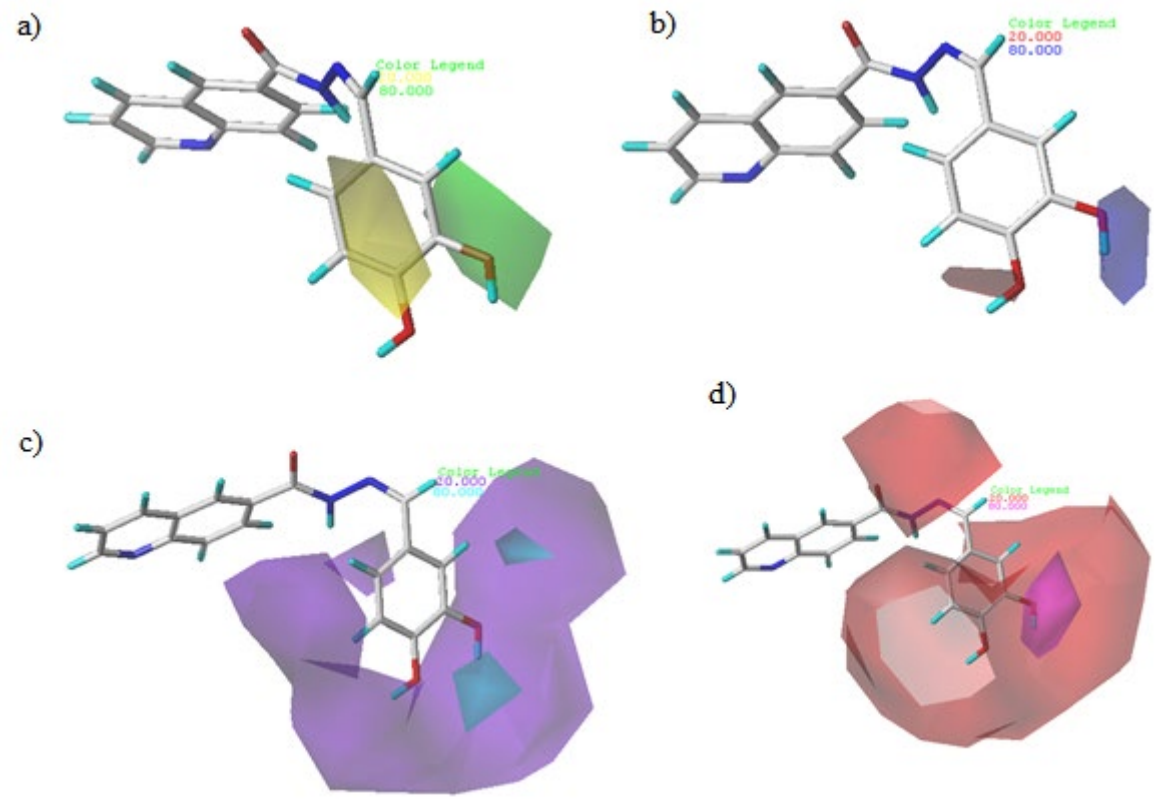

Fig. 4. CoMSIA/SEDA contour maps results. (a) Steric, (b) Electrostatic, (c**)** H-bond donor, (d) H-bond acceptor.

2.6 Summary of the SAR

In order to determine the appropriate groups for activity and thus propose new α-glucosidase inhibitors, the CoMSIA/SEDA contour maps were summarized as illustrated in **Fig. 5.** Specifically, the hydroxyl group found in the *meta* position of the phenyl group that requires bulky, electro-donating, H-bond donor and acceptor groups according to the results of CoMSIA/SEDA contour maps caught our attention to introduce suitable groups that can improve the α-glucosidase activity.

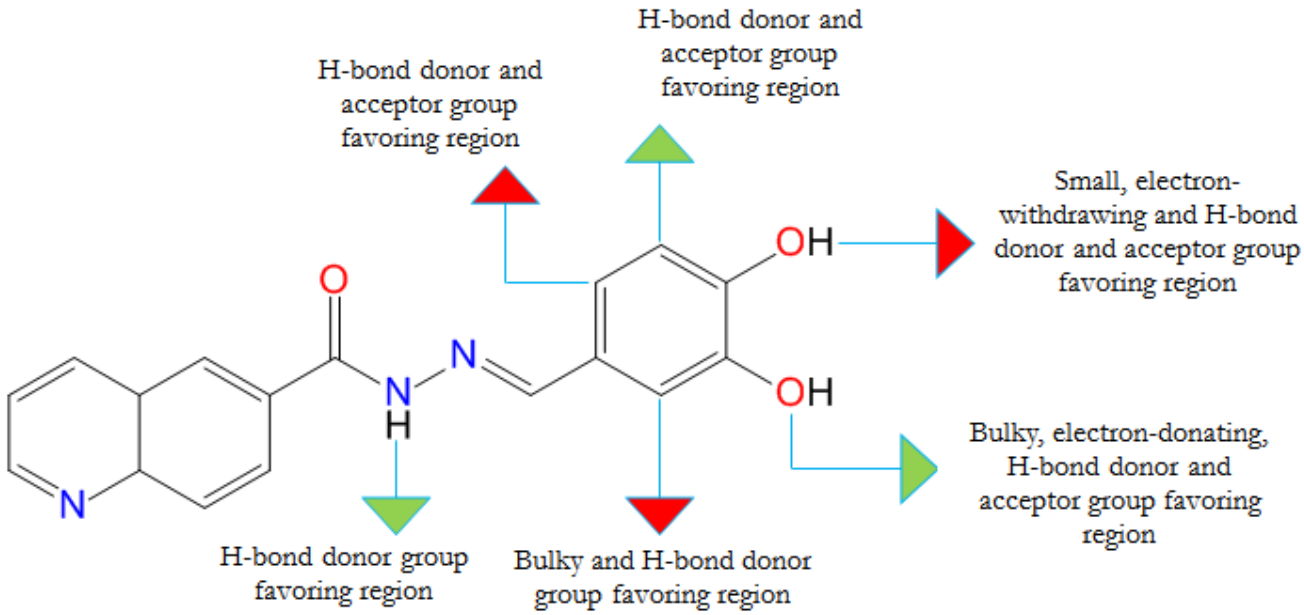

Fig. 5. Structural specifications for α-glucosidase inhibitors derived from the CoMSIA/SEDA contour map

2.7 New Molecules Design and α-Glucosidase Activity Prediction

The present study is intended at designing of new α-glucosidase inhibitors by studying the various structural characteristics extracted from the developed CoMSIA/SEDA model. Based on steric, electrostatic, hydrogen bond donor and acceptor contour maps findings, two new α-glucosidase inhibitors were suggested and their inhibitory activity pIC_{50} were predicted using the proposed CoMSIA/SEDA model as shown in **Table 7**. The phenyl group contains a hydroxyl group situated in the *meta* position was replaced by suitable groups such as isobutane and $N(Et)_2$, thus, new quinoline-based Schiff base compounds **E1** and **E2** were proposed with good α-glucosidase inhibiting activity. In fact, for compound **E1**, we substituted the -OH group with the isobutane moiety to improve steric hindrance, thereby increasing the α-glucosidase inhibitory activity. For compound **E2**, we replaced the -OH group by diethylamine ($N(Et)_2$) group in order to enhance the steric hindrance and electro-donating character. The chemical structures of the new designed molecules **E1** and **E2** are shown in **Fig. 6.**

Table 7. The predicted α-glucosidase inhibitory activity of the new molecules **E1** and **E1**.

Compound	Predicted pIC_{50}
	CoMSIA/SEDA
E1	5.244
E2	5.224

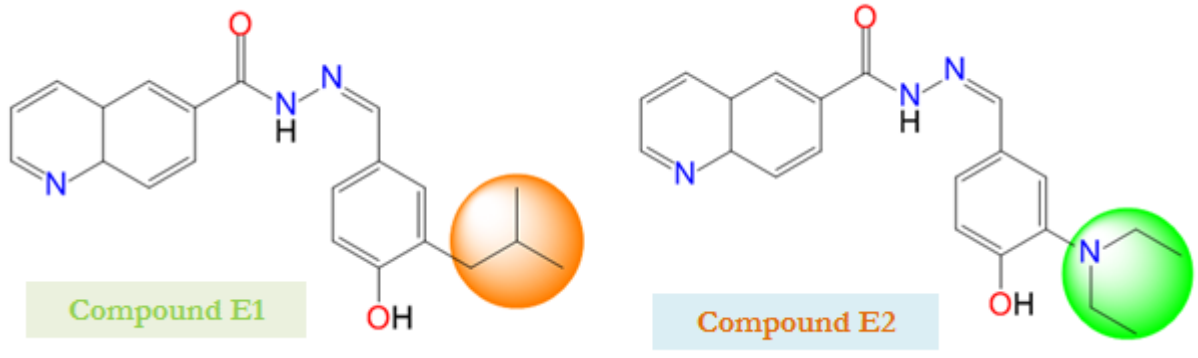

Fig. 6. Chemical structure of the proposed compounds **E1** and **E2.**

2.8 Drug Likeness Outcomes

The new α-glucosidase inhibitors **E1** and **E2,** and reference drug (voglibose), which is the most used α-glucosidase inhibitor in clinic, were subjected to further study using Lipinski's properties in order to identify their pharmacokinetics properties and to make a comparison between them. For this goal, we calculated the Lipinski's characteristics of the new proposed inhibitors and voglibose using pkCSM[35] and SwissADME[36] online servers and their properties are shown in **Table 8**. The Drug likeness prediction of the new inhibitors **E1**, **E2** and voglibose basing on Lipinski, Ghose, Veber and

Egan rules are shown in **Table 9**. **Table 8** provides clear evidence that the new α-glucosidase inhibitors have MW less than 500 Da, HBD not more than 5, HBA not over than 10. As a result, they can be easily absorbed and diffused.[37] On the other hand, voglibose has MW less than 500 Da, HBA not over than 10, but it has a HBD more than 5 revealing that this inhibitor can be hardly absorbed and diffused. Moreover, the molecules **E1** and **E2** have TPSA less than 140 Å and nrotb not more than 10 unlike to voglibose that has a TPSA value of 153.64 Å. So, the new compounds present a good bioavailability.[38] The synthetic accessibility of the newly proposed α-glucosidase inhibitors was evaluated to determine whether these compounds can be effectively synthesized or not. From **Table 8**, we can see that the molecules **E1** and **E2** have S.A values near to 1 and away from 10 unlike to voglibose. Therefore, these molecules can be easily synthesized (from 1 (simple to synthesize) to 10 (highly challenging to synthesize)).[39] Findings of **Table 9** exhibit that the new scaffolds are suitable to Lipinski rule, Ghose rule, Veber rule, and Egan rule unlike to voglibose that respects only Lipinski rule, thus, the new inhibitors **E1** and **E2** can be synthetized readily. These obtained findings exhibit the excellent bioavailability of the new recommended α-glucosidase inhibitors in comparison with voglibose.

Table 8. Lipinski's properties of newly the suggested molecules and reference drug.

property	Compound		
	E1	**E2**	Voglibose
MW	349.434	364.449	267.278
LogP	3.162	2.810	-4.492
HBA	4	5	8
HBD	2	2	8
nrotb	5	6	5
TPSA	74.05	77.29	153.64
SA	4.82	4.82	3.66
Abbreviations	**MW**: Molecular Weight, **HBA**: number of hydrogen bonds acceptors, **HBD**: number of hydrogen bonds donors, **LogP**: logarithm of partition coefficient of compound between n-octanol and water, **nrotb**: number of rotatable bonds, **TPSA**: Topological Polar Surface Area, **SA**: Synthetic accessibility		

Table 9. Drug likeness prediction of the new inhibitors and voglibose.

Compound	Lipinski	Ghose	Veber	Egan	Bioavailability Score
E1	Yes	Yes	Yes	Yes	0.55
E2	Yes	Yes	Yes	Yes	0.55
Voglibose	Yes	No	No	No	0.55

2.9 ADME Results

The primary obstacle encountered by researchers in the drug discovery domain involves identifying novel potent medications devoid of undesirable side effects. This is what prompted us to study the pharmacokinetics characteristics of the new recommended inhibitors. Therefore, pkCSM[35] and SwissADME[36] online servers were executed to predict the ADME properties of the new suggested compounds **E1** and **E2** as well as the reference compound (voglibose) as shown in **Table 10**. Regarding the water solubility of the studied molecules, the outcomes of **Table 10** point out that all α-glucosidase inhibitors are soluble. Absorbance value over than 30% of a molecule is considered to be highly absorbed.[40] The outcomes of **Table 10** clarify that the molecules **E1** and **E2** are very absorbed by the human intestine compared to the reference drug (voglibose). Moreover, if the distribution's size (VDss) value exceeds 0.45, it is thought to be large.[41] A blood-brain barrier (BBB) permeability is considered favorable when it exceeds 0.3, while it is deemed unfavorable if LogBB is below -1. The results of **Table 10** and **Fig. 7** clearly indicate the best distribution capability of molecules **E1** and **E2** compared to voglibose. Cytochrome P450s are believed to constitute the primary enzyme system responsible for drug metabolism within the liver.[42] Among humans, 17 families of CYP genes comprising a total of 57 genes have been identified. However, only the families CYP1, CYP2, CYP3, and CYP4 play a role in drug metabolism. Notably, CYP enzymes such as 2D6, 2C19, 2C9, 3A4, and 1A2 are responsible for more than 90% of medication biotransformation in phase I (oxidation) metabolism.[43] The two main cytochrome P450 subtypes are CYP3A4 and CYP2D6.[57] The findings of **Table 10** reveal that the studied α-glucosidase inhibitors are CYP3A4 substrate and not an inhibitor. The molecules **E1**, **E2** and voglibose are neither CYP2D6 substrate nor inhibitor. We can also note from the results in **Table 10** that the newly designed molecules are inhibitors of CYP1A2, CYP2C9 and CYP2C19 in contrast to the reference drug which is not an inhibitor of the three of CYP isoenzymes. Clearance is a parameter that establishes the connection between the concentration of a medication within the human body and the extent to which the medication is eliminated.[44] Certainly, lower clearance index values suggest that the drug remains in the body for a longer duration. The results obtained indicate that the new compounds possess a lower clearance index value in comparison to voglibose. This suggests that these compounds might exhibit a tendency to remain present in the human body for a prolonged period. The ADME outcomes of the molecules **E1** and **E2** demonstrate the good efficacy of these scaffolds and give them the priority to be candidate inhibitors against diabetes mellitus.

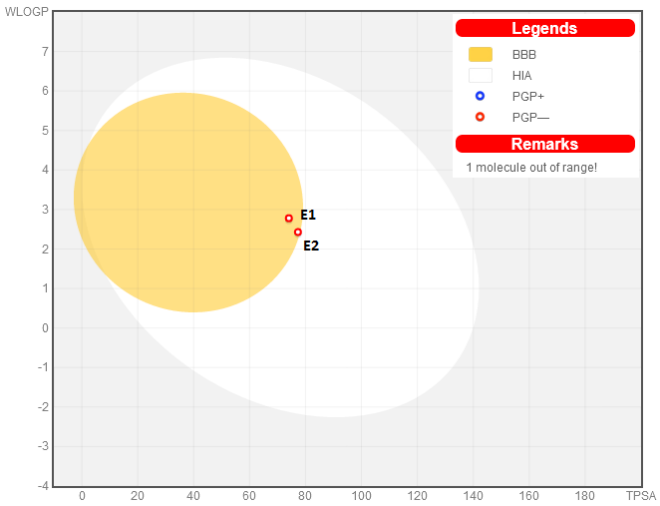

Fig. 7. BOILED-Egg model.

Table 10 ADME properties of the compounds **E1**, **E2** and voglibose.

N°	GI absorption		BBB permeant		P-gp inhibitor	CYP 1A2	CYP 2C19	CYP 2C9	CYP 2D6	CYP 3A4	CYP 2D6	CYP 3A4	Clearance
	High/ Low	Numeric (% absorbed)	Yes/No	Numeric (Log BB)	Yes/No	Inhibitor					Substrate		Numeric (log mL min^{-1} kg^{-1})
E1	High	91.144	Yes	0.011	No	No	Yes	No	No	Yes	No	Yes	0.716
E2	High	92.369	Yes	-0.351	No	No	Yes	No	No	Yes	No	Yes	0.829
Voglibose	Low	13.131	No	-1.870	No	No	No	No	No	No	No	No	0.913

2.10 Toxicity Result

The Ames mutagenicity test is a widely used assay in the early stages of drug development to evaluate the potential mutagenic effects of a molecule. Based on the outcomes listed in **Table 11**, the proposed molecules **E1** and **E2** as well as voglibose showed no toxicity according to the Ames test. Additionally, the studied molecules did not exhibit any carcinogenicity. Hepatotoxicity refers to the ability of a substance to cause damage or toxicity to the liver. It is an important aspect of toxicity testing, particularly for drugs and chemicals that are metabolized in the liver or have the potential to interact with liver cells. From **Table 11**, we can see that all inhibitors are not hepatotoxic. In a similar vein, the obtained outcomes hint that the proposed α-glucosidase inhibitors do not exhibit skin sensitisation. Moreover, based on the information provided in **Table 11**, it appears that the LD50 (lethal dose 50) values of the inhibitors are low. A low LD50 value indicates that a high dosage of the substance would be required to cause lethality in test subjects. In conclusion, the newly suggested α-glucosidase inhibitors demonstrate favorable pharmacokinetic properties and comply with Lipinski, Ghose, and Veber rules. These results indicate that these compounds could be promising candidates for the development of new inhibitors for diabetes mellitus.

Table 11 Toxicity prediction of the proposed molecules and voglibose.

Compound	Ames toxicity test	Carcinogenicity	Hepatotoxicity	Skin sensitisation	Oral Rat Acute Toxicity (LD50: mol/Kg)
E1	Non-toxic	Non-carcinogen	No-hepatotoxic	No	2.795
E2	Non-toxic	Non-carcinogen	No-hepatotoxic	No	2.806
Voglibose	Non-toxic	Non-carcinogen	No-hepatotoxic	No	1.611

2.11 Molecular Docking Results

2.11.1 Protein Structure Validation

The in-depth study conducted on the α-glucosidase protein (PDB ID: 3a4a) involved several analyses to assess the reliability of the selected receptor. These analyses included Asteroid plot analysis, Ramachandran plot, Z-Score plot, Verify 3D, and Error frequency plot. By performing these analyses on the α-glucosidase protein, we can gain insights into its structural quality, identify potential errors or irregularities, and determine the reliability of the receptor before conducting molecular docking analysis. These assessments contribute to ensuring the accuracy and validity of subsequent computational studies involving the protein. The Asteroid plot analysis conducted on the 3a4a receptor showed that the residues in the inner shell had direct contact with the ligand, while the residues in the outer shell had indirect interactions with the ligand. The size of the circular nodes in the plot corresponded to the number of contact residues formed with the

ligand (**Fig. 8(a)**). The subsequent analysis revealed that 89.1% of the tailings, when evaluated on the Ramachandran plot (**Fig. 8(b)**), were situated within the most favored region, indicating a high conformational quality of the protein. Additionally, the stereochemical validation was conducted using the ProSA server, which presented a graph displaying areas for X-ray crystallography and spectroscopy in light and dark blue, respectively. The Z-score obtained from this analysis was -10.43 (**Fig. 8(c)**), indicating good agreement between the protein structure and experimental data. Hence, the VERIFY3D graph exhibits that 98.12% of the residues had a 3D-1D score ≥ of 0.1, indicating a good model quality (**Fig. 8(d)**). The ERRAT graph analysis yielded a high estimated quality factor of 93.772 (**Fig. 8(e)**). This indicates a favorable overall quality assessment of the protein structure according to ERRAT. These validation tools provide assurance and reliability for the modeled protein structure, ensuring its suitability for conducting molecular docking studies.

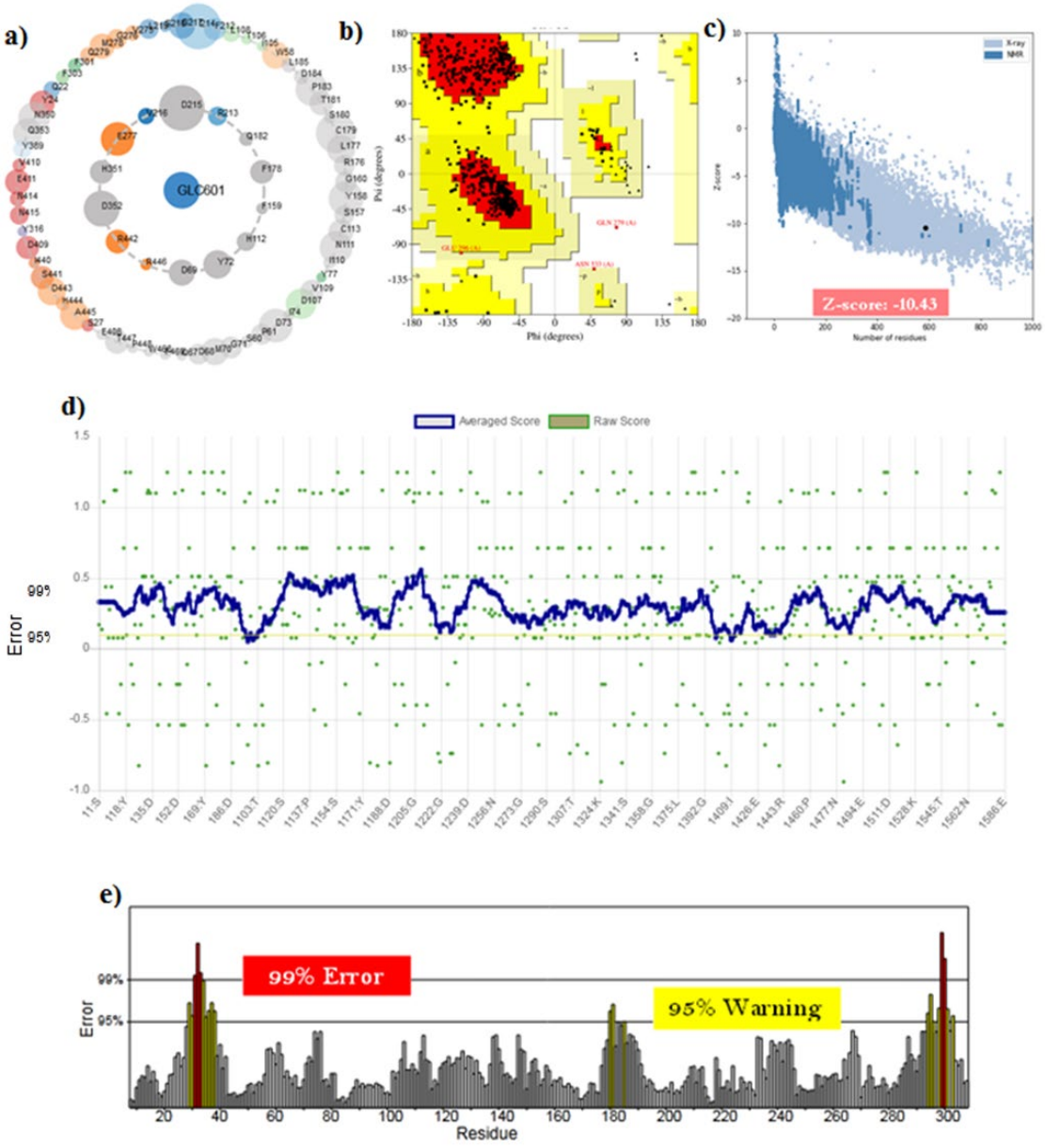

Fig. 8. Prediction and verification of the 3a4a receptor's structure encompass: a) Examination of the receptor through an asteroid plot analysis; b) Assessment of the Ramachandran plot using the pro check server; c) Presentation of the Z-Score plot for the modeled 3a4a structure; d) Evaluation of structural integrity using Verify 3D; e) Generation of an error frequency plot via the ERRAT server.

2.11.2 Molecular Docking Interaction

To better understand the different types of interactions of quinoline-based Schiff base inhibitors in the active site of the α-glucosidase receptor (PDB: 3a4a) and their binding affinity, a molecular docking simulation was applied. The compounds proposed in this study, **E1** and **E1**, as well as voglibose, clinically used as an α-glucosidase inhibitor, were docked into the active site of the target receptor. The binding energy and inhibition constant Ki values of the investigated molecules are presented in **Table 12**. Their molecular docking interactions are shown in **Figs 9, 10** and **11**, respectively. Based on the

obtained results, it was observed that inhibitors **E1** and **E2** exhibited the highest docking score against the receptor, surpassing the docking score of the reference inhibitor, voglibose. This suggests that compounds **E1** and **E2** have a stronger binding affinity and potentially better interaction with the active site of the receptor compared to voglibose. Additionally, the binding energy (ΔG) was used to calculate the inhibition constant (Ki) using the following equation $Ki = exp^{(\Delta G/RT)}$, where R is the universal gas constant (1.985 10-3 kcal mol^{-1} K^{-1}) and T is the temperature (298.15 K).[45] The results are listed in **Table 12**. Indeed, a lower Ki value indicates higher effectiveness of a drug. Ki represents the binding affinity between a drug and its target receptor. A lower Ki value implies stronger binding between the drug and the receptor, indicating greater potency and potentially improved therapeutic efficacy. Therefore, compounds **E1** and **E2** exhibit lower Ki values compared to voglibose, reinforcing their potential as more effective inhibitors of the α-glucosidase receptor.

The docking result of compound **E1** shows more favourable interactions with 3a4a receptor such as conventional hydrogen bond, pi-pi stacked and pi-pi T-shaped. Indeed, hydrogen bonds play a key role in determining the ligand's binding specificity. Furthermore, hydrogen bonds have a significant impact in drug-receptor interactions as well as maintaining the structural integrity of various biological molecules. These bonds contribute to the stabilization of the drug-receptor complex, facilitating optimal binding and enhancing the affinity and specificity of the interaction. One of the reasons why the proposed compound **E1** has the highest activity compared to the whole series may be due to its robust binding network. Continuously, the recommended **E1** molecule forms pi-alkyl interactions with the 3a4a receptor at residues Val216 (5.47 Å), Arg315 (5.45 Å), and Lys156 (3.93 Å). Other interactions were found to be pi-pi stacked, pi-sigma, alkyl, pi-anion and attractive charge with varying residues and distances. Compound **E2**'s docking outcome revealed four kinds of interactions with the active site residues. The hydroxyl group's oxygen atom in the phenyl ring established a hydrogen bond with active site residue Ser157 at distance of 2.54 Å. The quinoline ring's nitrogen atom forms a second hydrogen bond with the active site residue Arg442, positioned at a distance of 3.10 Å. The important number of H-bonds existing in the docking interaction of compound **E2** could explain its good stability. On the other hand, the docking result of voglibose showed two types of interactions. Voglibose molded four hydrogen bonds with active site residues Pro312 (2.36 Å), Asp242 (1.96, 2.41 and 2.42 Å), Ser240 (2.32 and 2.21 Å) and Ser241 (2.94 Å). These interactions provide the voglibose with good stability. As a conclusion, the molecular docking results provide support for the superiority of the new α-glucosidase inhibitors (compounds **E1** and **E2**) over voglibose. The higher docking scores and lower Ki values exhibited by compounds **E1** and **E2** suggest that they have stronger binding affinity and potentially better interactions with the active site of the α-glucosidase receptor compared to voglibose. These findings indicate that the new inhibitors may offer improved efficacy and effectiveness in inhibiting the α-glucosidase receptor, making them promising candidates for further development as potential therapeutics.

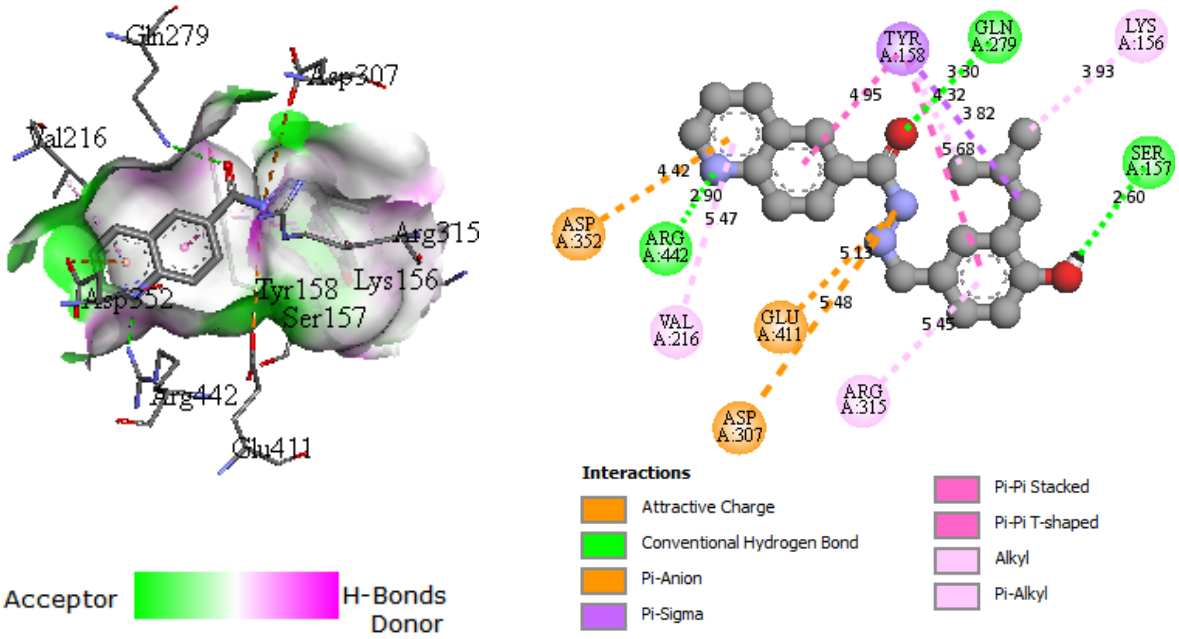

Fig. 9. Docking interaction of compound **E1** and 3a4a receptor (distance unit is given in angstrom Å)

Table 13 Binding energy and inhibition constant Ki of compounds **E1**, **E2** and voglibose

Inhibitor	Binding energy (Kcal/mol)	Inhibition Constant Ki (μM)
E1	-9.6	0.090
E2	-9.3	0.149
Voglibose	-6.4	20.116

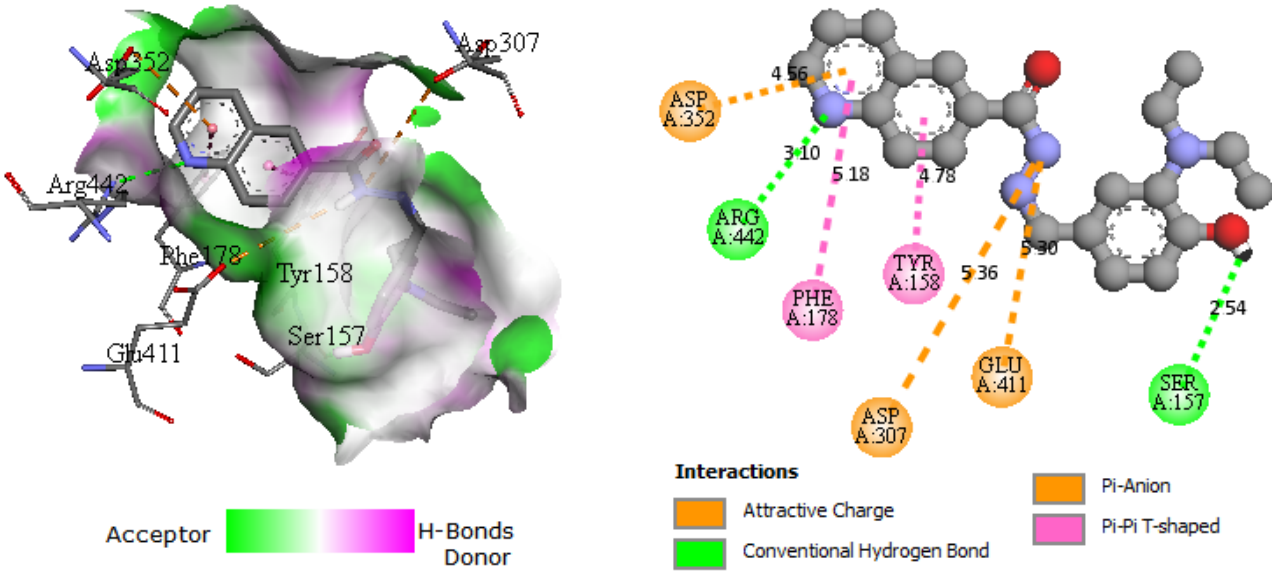

Fig. 10. Docking interaction of compound **E2** and 3a4a receptor (distance unit is given in angstrom Å)

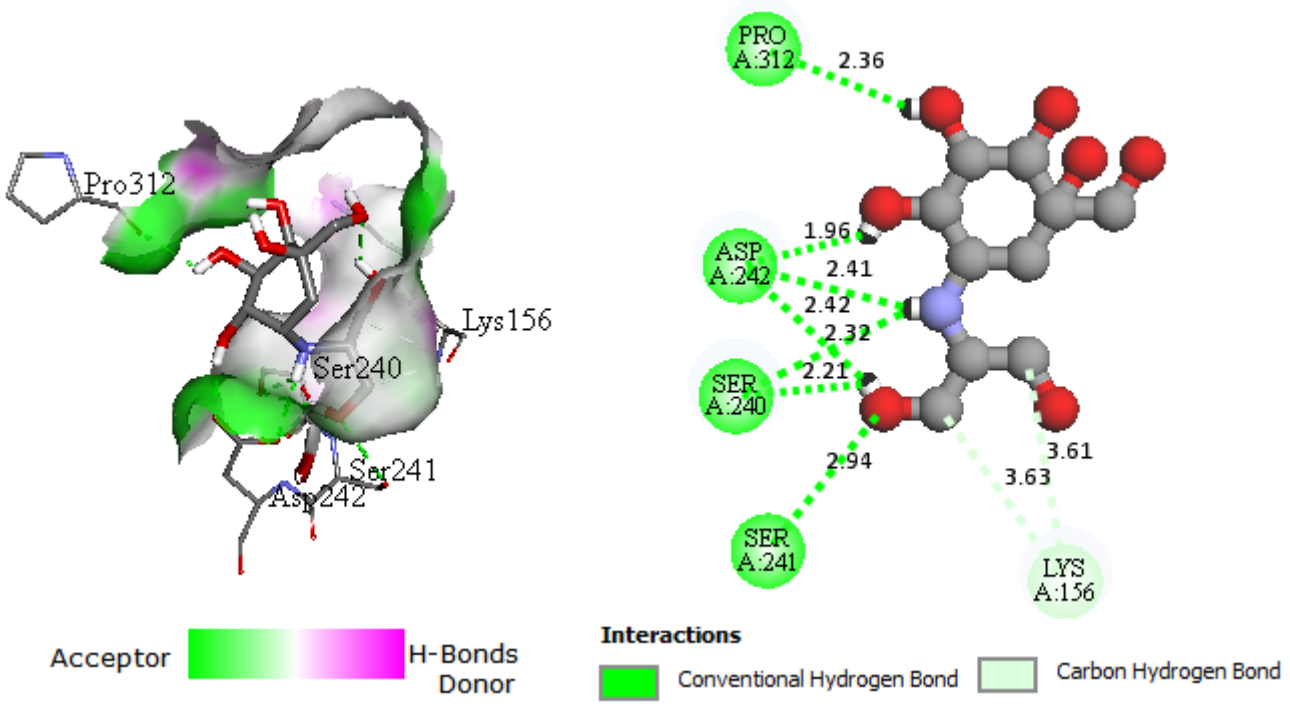

Fig. 11. Docking interaction of voglibose and 3a4a receptor (distance unit is given in angstrom Å)

2.11.3 Molecular Docking Validation Result

The re-docking was carried out to investigate the docking procedure and its efficiency. The re-docked complex was overlaid onto the co-crystallized native complex, as shown in **Fig. 12(a)**. The RMSD value obtained was 0.35 Å. In practice, the molecular docking validation is good if its RMSD value is less than 2 Å.[46] Thus, molecular docking using the Autodock Vina program was successfully validated in this study. Gln279, Arg442, Glu411 and Arg315 are the interacting amino acids formed with an average distance of 3.00 Å in the active site pocket (**Fig. 12(b)**).

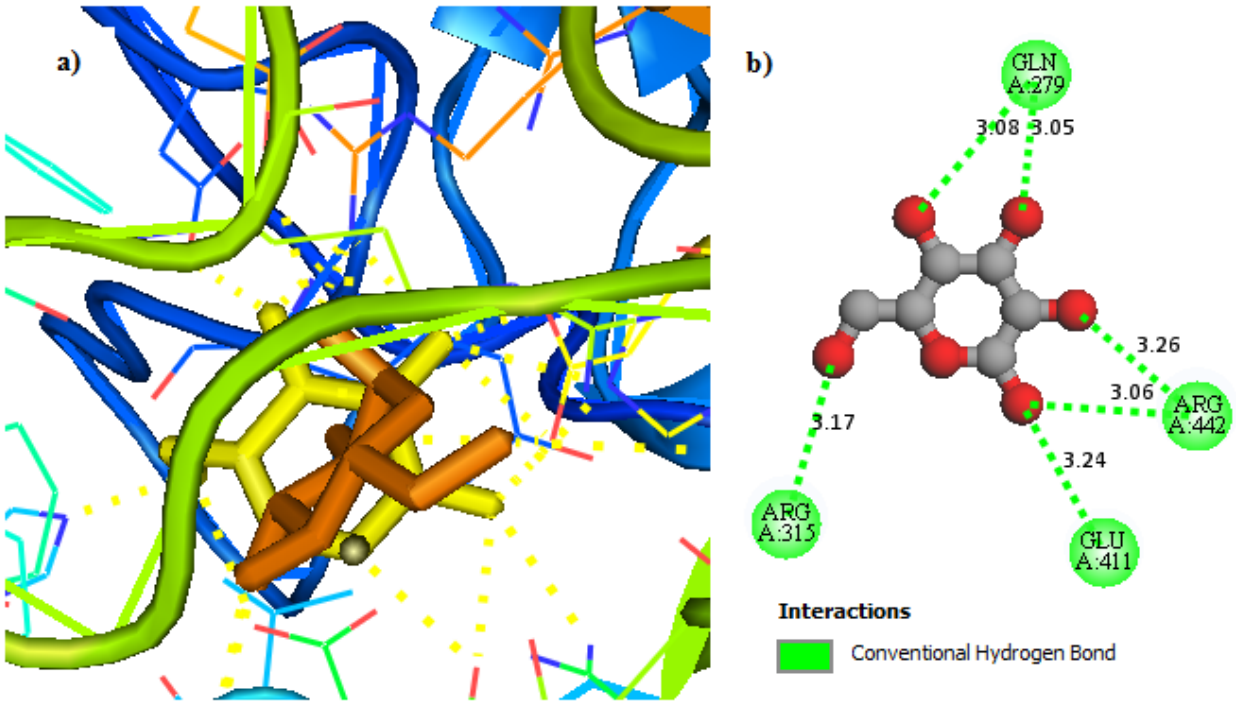

Fig. 12. a) Re-docking pose with the RMSD value of 0.35 Å (Yellow = Original, Orange = Docked), b) molecular docking interactions result of the original ligand.

2.12 MD Simulations Outcomes

The top three complexes involving 3a4a receptor and its associated ligands (E1, E2, and voglibose) were subjected to an assessment of their binding stability. This evaluation was conducted through a MD calculation involving simulations spanning 100 nanoseconds at standard room temperature conditions. Analysis of the trajectories after the simulation run indicated that, with the exception of the voglibose ligand, all other ligands remained attached to the ligand binding groove within the active pocket. To gauge the stability of each structure, various calculations were performed, including RMSD, RMSF, radius of gyration, hydrogen bonding analysis, determination of the average center of mass (COM) distance between the 3a4a protein and the concerned ligand, and estimation of binding free energy through MMPBSA. The RMSD graphs presented in (**Fig. 13, Column A**) illustrate the complex, backbone, and ligand RMSD across each structure. For both the protein backbone and complex RMSD, compounds E1 and E2 demonstrate minimal to no fluctuation after a simulation time of 40ns. In contrast, compound voglibose shows large values of RMSD and fluctuation for the complex and backbone RMSD plot. After almost 30ns of simulation time, trajectory visualization shows that ligand voglibose is out of its binding pocket. This is reflected in the RMSD plot by a huge increase in complex RMSD and intense fluctuations in ligand RMSD. The findings from the radius of gyration analysis (depicted in **Fig. 13, Column C**) align with the RMSD results for the complexes. Specifically, compounds E1 and E2 exhibit minimal fluctuations after 40 ns (less than 0.5 Å), while compound voglibose displays significant fluctuations with an increase exceeding 2 Å. The GROMACS program was employed to compute the RMSF for the protein complex, concentrating on 'C-alpha' atoms. In general, the magnitude of fluctuation remains under 3.0 Å for ligands E1 and E2, except for specific residues that correspond to protein loops or turns (illustrated in **Fig. 13, Column B**). Compound voglibose shows higher residue fluctuations compared with E1 and E2. This indicates that the ligand has a negative result on the stability of the protein unlike in E1 and E2 where lower residue fluctuations are observed. The count of hydrogen bonds established between the protein and ligand over the course of a 100 ns simulation is depicted in (**Fig. 14, Column A**). In the case of inhibitors E1 and E2, a notably stable network of hydrogen bonds with the protein is observed, with most of the simulation time involving the presence of two or one hydrogen bonds. Conversely, the voglibose ligand commences the simulation with a substantial number of hydrogen bonds established with the protein. However, it gradually loses all of these bonds after 30 ns of simulation, ultimately departing from the binding pocket. The average center-of-mass distance between the protein and ligand throughout the 100 ns simulation duration is illustrated in (**Fig. 14, Column B**). Ligands E1 and E2 stay within a reasonable COM distance from the protein while voglibose is out of its pocket completely and shows very high COM distance after 30 ns, in agreement with the previous results. The potential energy, temperature, and pressure values of the system extracted from the GROMACS edr file during the 100 ns MD simulation are depicted in **Fig. 15**. The graph demonstrates consistent and stabilized potential energy, temperature, and pressure profiles over the entire 100 ns simulation duration. The choice to employ the Molecular Mechanics/Poisson Boltzmann Surface Area (MM/PBSA) method for reevaluating complexes was driven by its speed as a force field-based approach to calculate binding free energy. This method is notably quicker compared to other computational techniques like free energy perturbation (FEP) or thermodynamic integration (TI) methods for estimating binding free energy. The g-

mmpbsa software was utilized to conduct the MM/PBSA calculation. The resulting binding free energies values are listed in **Table 13**.

Table 13 Binding free energies values of the suggested compounds and voglibose [kJ/mol]

Complex	ΔG	van der Waal energy	Electrostatic energy	Polar solvation energy	SASA energy
E1	-87.314 +/- 15.536	-146.567 +/- 20.675	-37.975 +/- 26.680	115.284 +/- 44.279	-18.055 +/- 1.615
E2	-77.207 +/- 17.801	-127.589 +/- 25.414	-45.660 +/- 21.933	112.517 +/- 31.617	-16.475 +/- 2.628
Voglibose	-53.753 +/- 81.767	-34.454 +/- 45.137	-58.394 +/- 72.513	44.063 +/- 119.266	-4.967 +/- 6.250

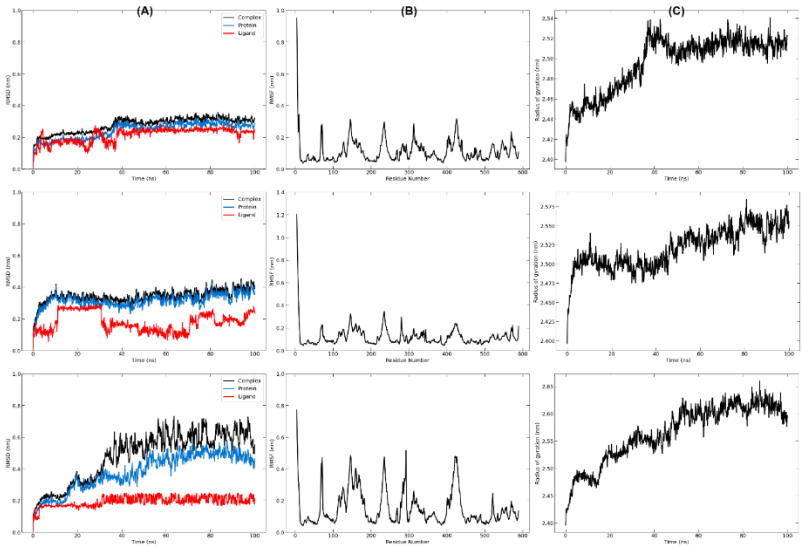

Fig. 13. In a sequence from right to left: (A) RMSD, (B) RMSF, and (C) Radius of gyration profiles of the complexes throughout a 100 ns MD simulation. Ligands **E1** (Top), E2 (Middle) and voglibose (bottom)

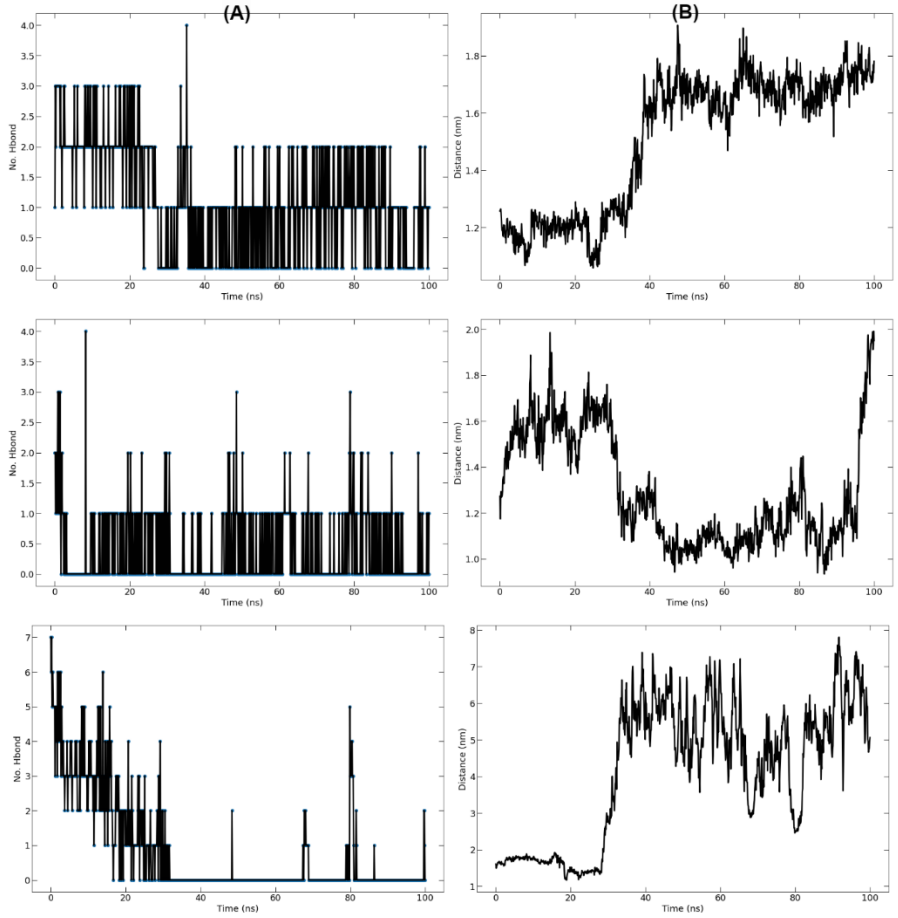

Fig. 14. Moving in a direction from right to left: (A) Illustration of hydrogen bonds between the protein and ligand, and (B) Presentation of the average distance between the ligand and the protein for the complexes over the course of a 100 ns MD simulation. Ligands **E1** (Top), E2 (Middle) and voglibose (bottom)

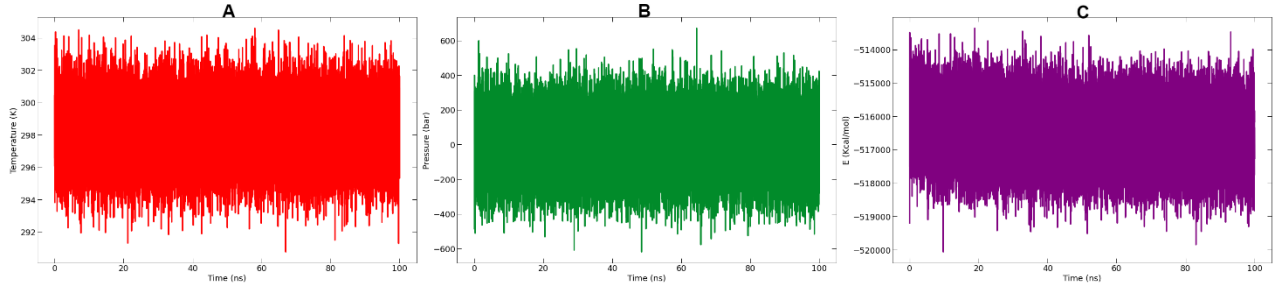

Fig. 15. In a progression from left to right: (A) Temperature variations, (B) pressure changes, and (C) potential energy fluctuations observed during the 100 ns MD simulations

2.13 Global Properties of the Quinoline-Based Schiff Base Derivatives

2.13.1 Frontier Molecular Orbital (FMO)

The highest occupied molecular orbital (HOMO) and the lowest unoccupied molecular orbital (LUMO) are crucial factors in quantum chemistry because they enable the study of chemical stability and reactivity and serve as the basis for the determination of global indices using Eqs. (9-13). The HOMO energy means the capacity to donate while the LUMO energy represents the acceptance characteristics of the investigated compound, thus requiring an electronic charge transfer from HOMO to LUMO.[47] Additionally, the energy gap (ΔEgap) refers to the difference in energy between the HOMO and the LUMO. The smaller the energy gap, the greater the reactivity and stability of the compound studied, according to the FMO theory. The HOMO, LUMO, and global reactivity descriptors results of the investigated compounds **E1** and **E2** are presented in **Table 14** while **Fig. 16** shows the isosurface and corresponding energy gap for the HOMO and LUMO orbitals. As can be seen in **Fig. 16,** compound **E1** has an energy gap value of 3.779 eV which is smaller than that of compound E2 (4.371 eV). This low value of the energy gap suggests that compound **E1** is, according to the FMO theory, the most reactive of the investigated compounds. Therefore, this finding supports the good α-glucosidase activity of compound **E1** predicted by the CoMSIA/SEDA model. Continuously, the electrophilicity ω index values of compounds **E1** and **E2** are 1.566 and 1.665 eV, respectively, while the nucleophilicity N index values are 4.038 and 3.367 eV, respectively. Hence, these compounds are considered potent nucleophiles rendering to the nucleophilicity scale [48] and weak electrophiles rendering to the electrophilicity scale.[49]

Table 14. HOMO-LUMO and global reactivity descriptors of the new α-glucosidase inhibitors.

	Global reactivity descriptors						
Compound	HOMO (ev)	LUMO (ev)	μ (ev)	η (ev)	**S** (ev)	ω (ev)	N (ev)
E1	-6.338	-2.138	-4.238	4.200	0.238	2.138	**3.030**
E2	-5.595	-2.076	-3.835	3.519	0.284	2.090	**3.773**

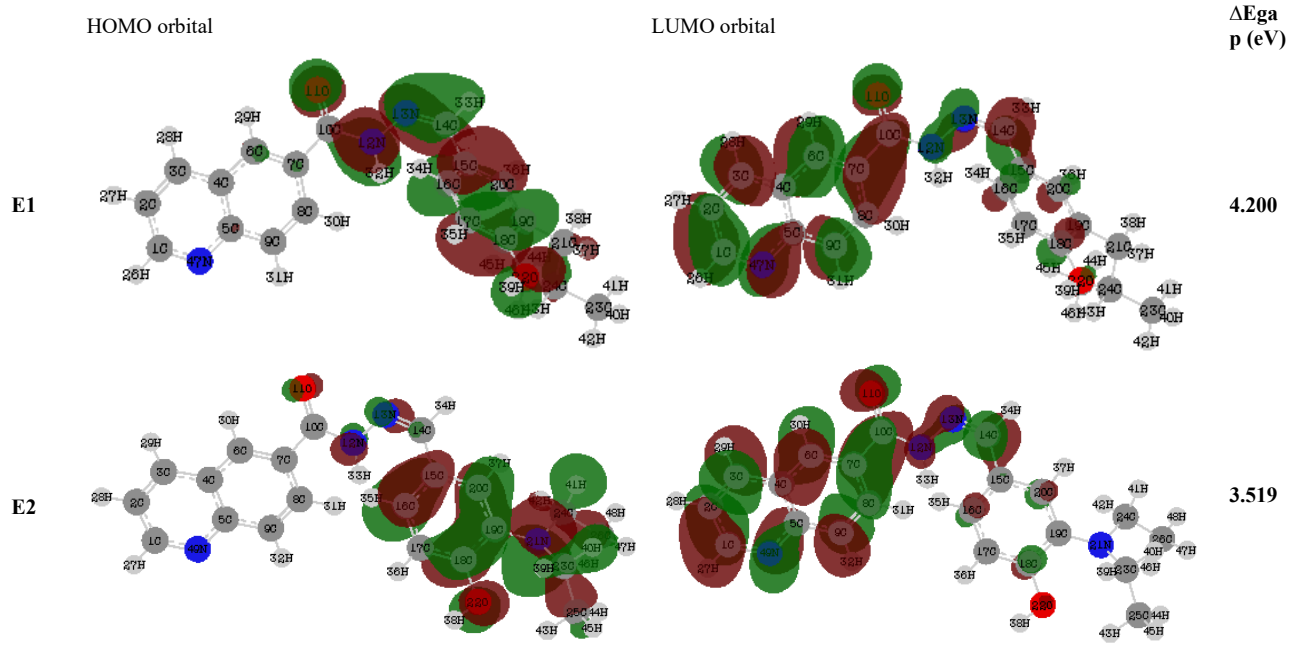

Fig. 16. HOMO, LUMO, and energy gap (ΔEgap) value of the compounds **E1** and **E2**.

2.13.2 Molecular Electrostatic Potential (MEP)

MEP describes the distribution of electrostatic potential energy in space around a molecule. It is determined based on the charges and positions of atoms within the molecule. MEP provides insights into the regions of positive and negative electrostatic potential, which are indicative of areas where molecules or functional groups might interact or undergo chemical reactions.[50] The MEP analysis is a valuable tool in understanding the electrostatic properties and behavior of molecules, aiding in the interpretation of chemical reactivity and molecular recognition. **Fig. 17** presents the analysis of MEP for the **E1** and **E2** compounds conducted using B3LYP functional with a 6-31G (d, p) basis set. In **Fig. 17**, the positive (electron-poor) regions are represented by the color blue, while the slightly electron-deficient regions are depicted in light blue. The neutral regions are shown in green, whereas the negative (electron-rich) portions are indicated by the color red. Additionally, the yellow color is used to represent regions that are slightly rich in electrons. This color scheme helps visualize the distribution of electron density and electrostatic potential around the studied compounds, allowing us to identify areas of electron deficiency and richness within the molecules. **Fig. 17** indicates that compounds E1 and E2 exhibit a strong negative potential (shown in red) at the O11 oxygen atom of the ketone group and a weaker negative potential (depicted in yellowish color) at the N13 nitrogen atom of the imine group. Hence, the regions with the highest negative electrostatic potential in **E1** and **E2** compounds are concentrated on the O11 and N13 atoms, indicating that these specific sites are the most favorable targets for electrophilic reactions.

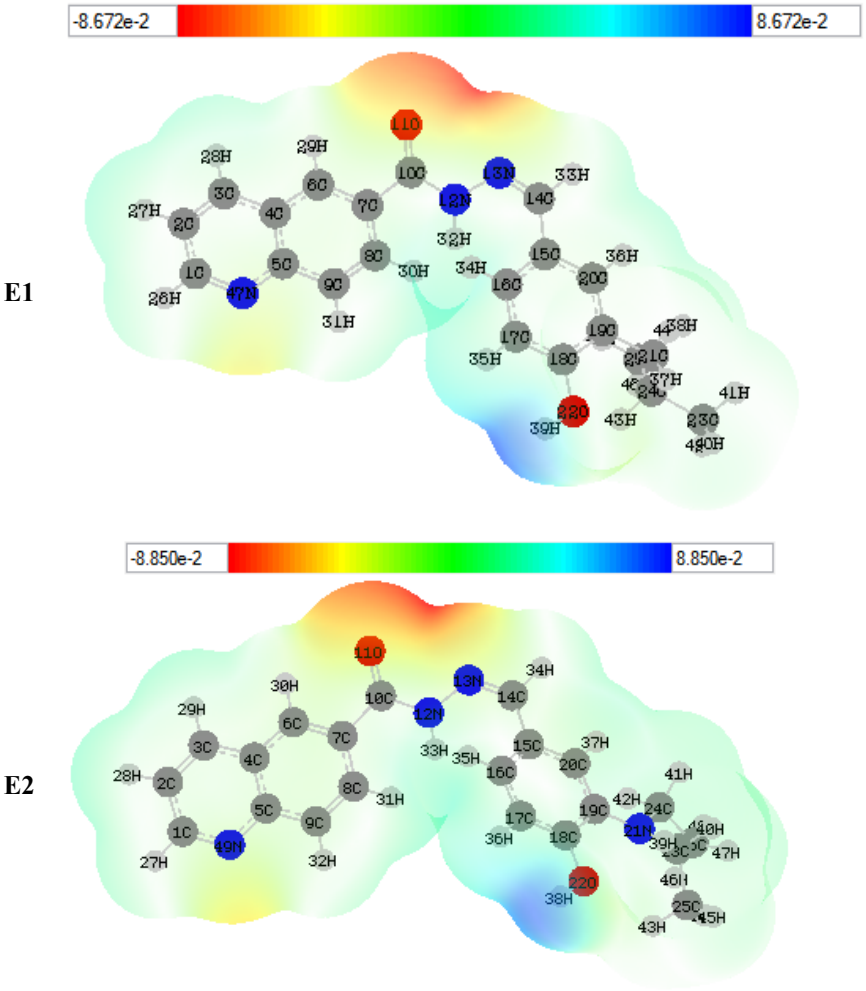

Fig. 17. Visual representation of the MEP diagrams.

2.14 Local Properties of E1 and E2 Inhibitors

In this part, local properties of **E1** and **E2** compounds were determined using P_k^+ and P_k^- Parr functions to identify the most nucleophilic and electrophilic centers. The obtained results are listed in **Table 15.**

It seems like the analysis of the electrophilic P_k^+ Parr function for the molecules **E1** and **E2** have revealed that the most electrophilic centers are the C6 and C15 atoms because they possess the highest values local electrophilicity index (ω_k). On the other hand, the nucleophilic P_k^- Parr function results for the molecule show that O11, N12, N13 and O22 are identified as the most nucleophilic centers since they exhibit the highest values of local nucleophilicity index (N_k).

Table 15. Local properties of compounds **E1** and **E2**.

Compound	Atom	P_k^+	P_k^-	ω_k	N_k
E1	C1	0.048	0.020	0.103	0.061
	C2	0.000	0.007	0.000	0.021
	C3	0.061	0.018	0.130	0.055
	C4	0.028	0.010	0.060	0.030
	C5	0.001	0.007	0.002	0.021
	C6	0.071	0.029	**0.152**	0.088
	C7	0.002	0.014	0.004	0.042
	C8	0.009	0.010	0.019	0.030
	C9	0.054	0.009	0.115	0.027
	C10	0.032	0.034	0.068	0.103
	O11	0.073	0.079	0.156	**0.239**
	N12	0.002	0.059	0.004	**0.179**
	N13	0.039	0.040	0.083	**0.121**
	C14	0.067	0.031	0.143	0.094
	C15	0.088	0.033	**0.188**	0.100
	C16	0.057	0.024	0.122	0.073
	C17	0.018	0.007	0.038	0.021
	C18	0.025	0.037	0.053	0.112
	C19	0.012	0.002	0.026	0.006
	C20	0.064	0.013	0.137	0.039
	C21	0.001	0.002	0.002	0.006
	O22	0.024	0.061	0.051	**0.185**
	C23	0.001	0.003	0.002	0.009
	C24	0.006	0.011	0.013	0.033
	C25	0.001	0.002	0.002	0.006
	N47	0.042	0.011	0.090	0.033
E2	C1	0.048	0.012	0.100	0.045
	C2	0.000	0.005	0.000	0.019
	C3	0.063	0.009	0.132	0.034
	C4	0.029	0.006	0.061	0.023
	C5	0.002	0.001	0.004	0.004
	C6	0.072	0.019	**0.150**	0.072
	C7	0.002	0.007	0.004	0.026
	C8	0.001	0.003	0.002	0.011
	C9	0.054	0.006	0.113	0.023
	C10	0.033	0.019	0.069	0.072
	O11	0.073	0.05	0.153	**0.189**
	N12	0.033	0.046	0.069	**0.174**
	N13	0.036	0.035	0.075	**0.132**
	C14	0.066	0.017	0.138	0.064
	C15	0.091	0.011	**0.190**	0.042
	C16	0.031	0.010	0.065	0.038
	C17	0.015	0.018	0.031	0.068
	C18	0.017	0.003	0.036	0.011
	C19	0.029	0.011	0.061	0.042
	C20	0.051	0.011	0.107	0.042
	N21	0.014	0.016	0.029	0.060
	O22	0.017	0.030	0.036	**0.113**
	C23	0.007	0.011	0.015	0.042
	C24	0.008	0.020	0.017	0.075
	C25	0.001	0.006	0.002	0.023
	C26	0.004	0.013	0.008	0.049
	N49	0.032	0.0229	0.067	0.086

3. Conclusion

The outcomes of this research likely offered valuable information for the development of new α-glucosidase inhibitors. This could involve studying the SAR of existing inhibitors, identifying key features that contribute to their effectiveness, and using that knowledge to develop new compounds with enhanced properties. The optimal HQSAR/A-B-C-H-Ch-DA and CoMSIA/SEDA models showed good statistical findings regarding numerous stringent statistical indicators like Q^2, R^2 and R^2pred. Thus, these models can be competently applied to predict new α-glucosidase inhibitors with excellent activity. The contour maps results displayed that steric, electrostatic and hydrogen bond acceptor groups were found to be useful for improving the α-glucosidase inhibitory activity. Overall, these outcomes pave the way to design two novel α-glucosidase inhibitors with high activity compared to that of the more active molecule of the series. ADME/Tox outcomes of the predicted α-glucosidase inhibitors showed good absorption, acceptable metabolism transformation, and they were in great accordance with the key principles rules of drug likeness compared to the reference medication (voglibose). Molecular docking outcomes showed good stability of the new suggested inhibitors at the active pocket of α-glucosidase receptor. The molecular dynamics simulations conducted during the research demonstrated that the new α-glucosidase inhibitors exhibited

good stability during the 100 ns simulation. The application of DFT analysis in the study allowed for the identification of both electrophilic and nucleophilic inhibitors, along with determining the specific sites that are most favorable for nucleophilic or electrophilic interactions. This study indicates that the newly suggested α-glucosidase inhibitors have significant potential for treating type-2 diabetes mellitus in the future. However, additional *in vitro* and *in vivo* investigations are needed to thoroughly evaluate their therapeutic efficacy.

Acknowledgements

We are grateful to the "Association Marocaine des Chimistes Théoriciens" (AMCT) for its pertinent help concerning the programs.

4. Experimental

4.1. Materials and Methods

4.1.1 Dataset

In this study, the *α*-glucosidase inhibitory activity and chemical structures of seventeen quinoline-based Schiff base derivatives were taken from literature.[51] The selected molecules were synthetized by Taha et al. from simple methods and substrates, and assessed for their *α*-glucosidase inhibitory activity.[51] These compounds were divided into two groups and employed for conducting the 3D-QSAR (CoMSIA) analysis. The first group concerned with a training set of 13 compounds to construct the quantitative model and the second one concerned with a test set of 4 compounds to verify the effectiveness of the shaped model. The *α*-glucosidase inhibitory activities IC_{50} (μM) were transFig.d into the equivalent pIC_{50} (-log (IC_{50})) values (**Table 16**). **Fig. 18** shows the chemical structure of the seventeen investigated molecules.

Table 16. *α*-Glucosidase activity of the studied compounds and their chemical structures.

N°	R	IC_{50}	pIC_{50}	N°	R	IC_{50}	pIC_{50}	N°	R	IC_{50}	pIC_{50}
1	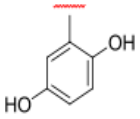	12.4	4.907	**7** [a]	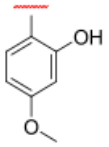	21.6	4.666	**13**	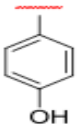	23.5	4.629
2	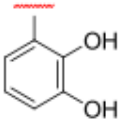	9.4	5.027	**8**	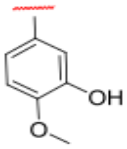	14.4	4.842	**14**	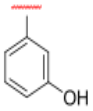	13.2	4.879
3	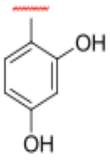	14.1	4.851	**9**[a]	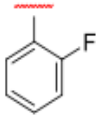	7.4	5.131	**15**	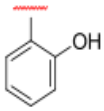	35.7	4.447
4	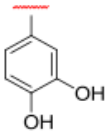	6.2	5.208	**10**	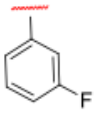	48.2	4.317	**16**	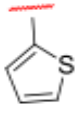	28.6	4.544
5 [a]	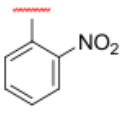	37.6	4.425	**11**	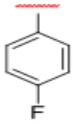	28.9	4.539	**17**	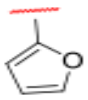	38.45	4.415
6 [a]	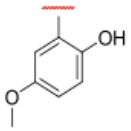	18.4	4.735	**12**	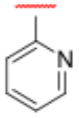	38.4	4.416				

[a] *Test set molecules*

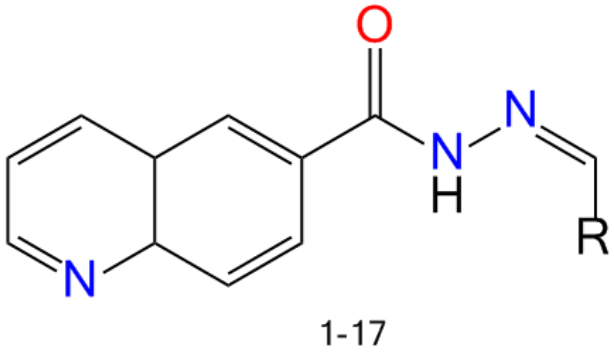

Fig.18. General structure of quinoline-based Schiff base molecules.

4.2 Minimization and Molecular Alignment

Alignment of molecules is a crucial initial step applied before building a 3D-QSAR molecular model. In this paper, every structure of seventeen quinoline-based Schiff base molecules were sketched with SYBYL-X.2.0 and minimized using the Tripos force,[52] Gasteiger Huckel charges,[53] and with gradient convergence criteria of 0.005 kcal/mol. Then, using compound **C4** (the database's more active inhibitor), the seventeen concerned derivatives were aligned on the common core as shown in **Fig. 19**.

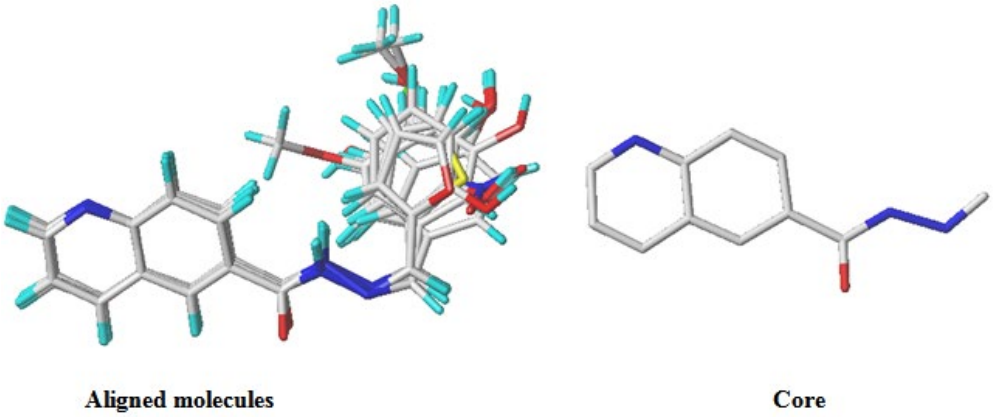

Fig. 19. The proposed alignment of the seventeen quinoline-based Schiff base molecules.

4.3 HQSAR Study

The hologram QSAR is a 2D-QSAR method that establishes a relationship between the biological activity of a compound and its structural fragments.[54] This technique involves converting the chemical representation of a compound into its equivalent molecular hologram. One of the key advantages of hologram QSAR is that it eliminates the need for a 3D structure, molecular alignment, and the specification of conformation.[55] This makes hologram QSAR a valuable tool in predicting biological activity based on the compound's structural features in a simplified and efficient manner. Molecular holograms are generated through a process called fragment generation, which involves hashing the fragments into an array. The bin occupancies within the array are used as descriptor variables.[56] To generate molecular holograms, the HQSAR technique utilizes a range of parameters, including fragment distinction of atoms (A), bonds (B), connections (C), hydrogen atoms (H), chirality (Ch), donor and acceptor (DA), hologram length (HL) values of 53, 59, 61, 72, 83, 97, 151, 199, 257, 307, and 401. Additionally, the fragment sizes considered are 2-5, 3-6, 4-7, 5-8, 6-9, and 7-10. These parameters play a crucial role in defining the characteristics of the molecular holograms and are essential for the HQSAR technique's predictive capabilities in relating structural features to the compound's biological activity.

4.4 CoMSIA and PLS Analyses

CoMSIA[31] is a computational method used in drug design to study the 3D-QSAR of a set of compounds. In CoMSIA analysis, the steric, electrostatic, hydrophobic, hydrogen bond donor, and hydrogen bond acceptor fields are used to describe the properties of the molecules being studied. These fields represent different physicochemical properties that influence the biological activity of the inhibitors. The combination between these fields leads to produce a CoMSIA model. Regarding the attenuation factor in CoMSIA, it regulates the steepness of the Gaussian function used to weight the contributions of different interactions between molecules. The default value of the attenuation factor is set to 0.3.

The partial least squares (PLS) [57] approach has been applied to setting up a linear relationship between the values of α-glucosidase activities and the CoMSIA descriptor. As a matter of fact, PLS using a leave-one-out (LOO) cross-validation was executed to offer the cross-validated Q^2 and optimum number of components (N). Afterwards, PLS approach was re-effectuated using this time a non-cross-validation to engender the determination coefficient R^2, F values and standard error of estimate (SEE). The optimal CoMSIA model was chosen by taking into account the best Q^2, R^2, and R^2pred values.

4.5 External Validation of 2D/3D-QSAR Model

A study by Golbraikh and Tropsha suggests that cross-validation is necessary but not enough to check the predictive capability of the nominated QSAR mode.[58] However, an external validation using a set of tests molecules can provide a guarantee of the predictive potential of the molded model. In fact, to assess the predictive capability of the model, the predictive correlation coefficient (R^2pred) was identified using the formula (1)[58]:

$$R^2\text{pred} = 1 - \frac{\text{PRESS}}{\text{SD}} \tag{1}$$

where the PRESS parameter refers to the squared deviations between the calculated and observed activity values of the compounds in the test set, and the SD parameter represents the squared deviations between the average activity values of the training set and the activity values of the test set. Furthermore, Golbraikh and Tropsha[58] determined additional statistical factors including the squared correlation coefficients r_0^2 and $r_0'^2$, and the slopes k and k′ for an additional statistical analysis regarding the external validation. These parameters were computed using the Eqs. (2-4), and Eq. (5), respectively:

$$r_0^2 = 1 - \frac{\sum(Y_{\text{pred/test}} - k \times Y_{\text{pred/test}})^2}{\sum(Y_{\text{pred/test}} - k \times \overline{Y}_{\text{pred/test}})^2} \tag{2}$$

$$r_0'^2 = 1 - \frac{\sum(\overline{Y}_{\text{pred/test}} - k \times \overline{Y}_{\text{pred/test}})^2}{\sum(Y_{\text{pred/test}} - k \times Y_{\text{pred/test}})^2} \tag{3}$$

$$k = \frac{\sum(Y_{\text{test}} \times Y_{\text{pred/test}})^2}{\sum(Y_{\text{pred/test}})^2} \tag{4}$$

$$k' = \frac{\sum(Y_{\text{pred/test}} \times Y_{\text{test}})^2}{\sum(Y_{\text{test}})^2} \tag{5}$$

An investigation carried out by Roy[59] demonstrated that it is compulsory to calculate the parameters r_m^2 and $r_m'^2$, which are the distinction between r^2 and r_0^2 values, r^2 and $r_0'^2$ values, respectively to ensure the efficiency of the model and thus could be considered for the prediction of the activity of newly put forward compounds. r_m^2 and $r_m'^2$ parameters are calculated using the Eq. (6), and Eq. (7), respectively:

$$r_m^2 = r^2\left(1 - \sqrt{(r^2 - r_0^2)}\right) \tag{6}$$

$$r_m'^2 = r^2\left(1 - \sqrt{(r^2 - r_0'^2)}\right) \tag{7}$$

4.6 New Molecules Design and α-Glucosidase Activity Prediction

The primary objective of this research is to design novel α-glucosidase inhibitors with important inhibitory activity. To achieve this goal, the HQSAR/CoMSIA model was constructed, validated, and subsequently employed to generate HQSAR/CoMSIA contribution and contour maps. These maps offer valuable understandings regarding the structural characteristics and regions that significantly influence the inhibitory activity of the designed compounds, aiding in the rational design and optimization of new potential inhibitors. The newly designed molecules underwent sketching, minimization, and alignment using the same procedure as the seventeen previously studied molecules. The α-glucosidase activity of the newly designed quinoline-based Schiff base molecules was forecasted using the most reliable and well-established HQSAR/CoMSIA model.

4.7 ADME/Tox Prediction

ADME/Tox (absorption, distribution, metabolism, excretion, and Toxicity) prediction has emerged as a fundamental and extensively employed approach in molecular modeling to assess the pharmacokinetic characteristics of molecules.[60] This predictive tool plays a crucial role in understanding how a compound is absorbed, distributed, metabolized, and

eliminated in the body, as well as its potential toxicity.[61] It aids in the early stages of drug discovery and development by providing valuable information about a molecule's behavior within the human body, facilitating the identification of potential drug candidates with favorable ADME/Tox profiles. Keeping this in mind, we used pkCSM[35] and SwissADME[36] online servers to predict the ADME/Tox parameters of the newly designed candidate scaffolds.

4.8 Molecular Docking Analysis

Molecular docking was carried out to explore and analyze the possible interactions between molecules and the receptor. The protein data for isomaltase from Saccharomyces cerevisiae's crystal structure was sourced from the Protein Data Bank with the PDB ID: 3a4a [2,62] and a resolution of 1.60 Å. A grid box with dimensions x = 30, y = 30, and z = 30 was established within the binding pocket of the 3a4a receptor. The grid points were spaced 1 Å apart from each other. The parametric dimensions of the grid box were set as follows: x = 21.595, y = -7.436, and z = 24.042. To achieve an effective pose of the binding conformation of the 3a4a- quinoline-based Schiff base complex, the exhaustiveness value was set to 8. Next, the recommended molecules **E1** and **E2**, and voglibose, clinically used as α-glucosidase medication, were docked against the target protein. In this part, Autodock Vina[63] was applied to conduct the docking simulation. AutoDock Vina produced distinct docked complexes for each ligand, varying in conformation and affinity scores (measured in kcal/mol). These complexes were categorized based on the theory of lowest binding energy (in kcal/mol), where a more negative value indicates a higher binding affinity.[64] The best pose of the docked protein-ligand complex was analysed and visualized graphically using Discovery Studio 2016[65] and PyMol[66] software.

4.9 Molecular Docking Validation

The molecular docking method was validated to assess its credibility. The co-crystalized molecule was retired and re-docked into the active site using Autodock Vina.[63] It was docked using the same technique and steps as those adopted for the docked ligands studied. The re-docked complex was superimposed on the co-crystallized reference complex using PyMol[66] and the root mean square deviation (RMSD) was computed, and the two-dimensional picture displaying the superimposed amino acid residues was visualized using the Discovery Studio 2016 software.[65]

4.10 Molecular Dynamics (MD) calculations

4.10.1 MD calculations

The best docking poses of the 3a4a-E1/E2/voglibose complex were subjected to MD calculations to further understand their stability. The system was constructed using the web-based CHARMM-GUI,[67,68] which was integrated with the CHARMM36 force field.[69] The ligand topology was generated using the general CHARMM force field[70] through the Param-Chem server. There are five sequential stages comprising the construction process of the CHARMM-GUI solution. In the initial stage, the tool reads the coordinates of the protein-ligand complex. In the next step, the protein-ligand complex is solvated, and the size of the system and structure are defined. During this step, the Na+ and Cl^- ions were used to neutralize the system. The third step involves setting up periodic boundary conditions (PBC), which simulate an extensive system by repeating a unit cell in all directions. Only the atoms within the PBC box are included in the MD simulation. At this stage, a rapid minimization is performed to remove any unfavorable contacts. The fourth and fifth stages include system equilibration and the production phase. Equilibration is carried out in two phases—first using the NVT ensemble and then the NPT ensemble—to guarantee that the system achieves the required temperature and pressure. Subsequently, necessary adjustments, such as modifying the number of steps in an MD run, the frequency of trajectory saves, and energy calculations, are made to the input files for equilibration and production. GROMACS 2020.2 was used for all MD calculations, including both the equilibration and production runs. To counterbalance the overall atomic charge of the entire system, a procedure involving the introduction of Na^+ and Cl^- ions, as well as the random substitution of water molecules, was employed subsequent to the initial solvation of all complexes within a cubic TIP3P water box.[71] Periodic boundary conditions (PBC) were applied with consideration for the system's size and shape. Unbound interactions were managed using a 12 Å cut-off distance, and the Verlet cut-off strategy was employed to buffer the neighbor search list. The Particle-Mesh Ewald (PME) technique was used to handle long-range electrostatic interactions.[72] The complexes under study were subjected to the CHARMM36 force field.[69] Before commencing the production simulation, the system's energy was reduced through minimization using the steepest descent algorithm, which involved 5000 iterative steps. The chosen complexes were subsequently exposed to NVT and NPT ensembles, simulating a duration of 125 ps at a temperature of 300.15 K. During this process, positional constraints of 400 kJ mol^{-1} nm^2 and 40 kJ mol^{-1} nm^2 were applied to the backbone and side chains, respectively. These constraints aimed to achieve equilibrium and stabilize both temperature and pressure. The complexes are then put through a 100 ns production simulation in an NPT ensemble at 300.15 K and 1 bar. The Nose-Hoover thermostat was employed to control the temperature and the Parrinello-Rahman barostat to maintain the pressure. The LINCS algorithm was used to constrain H-bonds based on inputs from CHARMM-GUI. This was achieved using the V-rescale thermostat set at 300 K with a coupling constant of 1 ps. Trajectories were saved and recorded at intervals of every two ps. During the production phase, simulations were put into practice using the NPT ensemble and extended for a duration of 100 ns.

4.10.2 Analyzing Trajectories

GROMACS software tools were utilized to assess and analyze the outcomes of the MD simulations. The RMSD of both ligand and protein atom positions was calculated by aligning the protein backbone atom using the gmx_rms subprogram. Also, the same subprogram was used to compute the root mean square fluctuations (RMSF) based on the C-alpha atoms of the protein. The gmx_gyrate tool was used to determine the radius of gyration (Rg) for all protein atoms, while the determination of the count of hydrogen bonds present in the interface between the protein and the ligand was carried out using the gmx_hbond utility. During the simulation, the gmx_distance tool was utilized to compute the center of mass distance separating the protein and the ligand. The visualization of trajectories and the analysis of protein-ligand contact frequency were put into practice using the VMD molecular graphics software.

4.10.3 Binding Free Energy using MM/PBSA Approach

The g_mmpbsa utility in GROMACS, used to evaluate predicted binding affinity, was employed to conduct MM/PBSA (Molecular Mechanics/Poisson-Boltzmann Surface Area) computations for the systems chosen for further analysis. In a general sense, the formula (8) below can be used to describe the free energy of binding between the protein and the ligand in the presence of a solvent:

$$\Delta G_{binding} = \Delta G_{complex} - (\Delta G_{protein} + \Delta G_{ligand}) \quad (8)$$

In this context, the $\Delta G_{complex}$ parameter refers to the overall free energy of the protein-ligand complex, while $\Delta G_{protein}$ and ΔG_{ligand} parameters indicate the combined free energies of the isolated protein and ligand within the solvent, respectively. Additionally, it is possible to compute the energy contributed by each residue to the binding energy using the tool g_mmpbsa. To decompose the binding energy, ΔE_{MM}, ΔG_{polar} and $\Delta G_{non-polar}$ were initially calculated separately for each residue, and then summed to determine each residue's contribution to the overall binding energy. Since g_mmpbsa can only read files from specific GROMACS versions, GROMACS 5.1.4 was used to create a new binary run input file (.tpr) required for MM-PBSA calculations with g_mmpbsa. The MD process produced the necessary files to generate this binary run input file: a molecular structure file (.gro), a topology file (.top), and an MD parameter file (.mdp).

4.11 Global and Local Properties of the Quinoline-Based Schiff Base Derivatives

An additional computational investigation of the quinoline-based Schiff base derivatives using the Density Function Theory (DFT) approach and the Gaussian G09 package[73] on the B3LYP/6-31G (d,p) basis set was carried out to reach the equilibrium geometry of each compound. Based on the well-known Koopmans approximation, quantum chemical computations were done to determine the global reactivity electronic descriptors.[74] Therefore, the global reactivity descriptors were computed using Eqs. (9-13):

$$\mu = (E_{HOMO} + E_{LUMO})/2 \quad (9)$$
$$\eta = E_{LUMO} - E_{HOMO} \quad (10)$$
$$S = 1/\eta \quad (11)$$
$$\omega = \mu^2/2\eta \quad (12)$$
$$N = E_{HOMO}(Nu) - E_{HOMO}(TCE) \quad (13)$$

where μ, η, S, ω, and N are the chemical potential, chemical hardness, chemical softness, electrophilicity, and nucleophilicity, respectively. Furthermore, by examining the atomic spin density (ASD) at the radical anion and radical cation, it is possible to observe the electron density distribution in the nucleophile and electrophile as they come closer to each other during the reaction. Considering these results, Domingo presented the Parr functions P(r),[74] which are expressed through the Eq. (13) and Eq. (14):

$$P_k^- = \rho s^{rc}(r) \quad \text{for electrophilic attacks} \quad (14)$$
$$P_k^+ = \rho s^{ra}(r) \quad \text{for nucleophilic attacks} \quad (15)$$

where $\rho s^{rc}(r)$ denotes the ASD at the radical cation's r atom and $\rho s^{ra}(r)$ denotes the ASD at the radical anion's r atom for a given molecule. Local electrophilic P_k^+ and nucleophilic P_k^- Parr functions of the neutral compound are afforded by each ASD collected at the various atoms of the radical cation and anion of a compound.
The equations (16) and (17) define the local electrophilicity ω_k[75] and local nucleophilicity N_k[49] indices, respectively. These indices enable the dispersion of the overall electrophilicity ω and nucleophilicity N indices to the specific atomic positions denoted as (k).

$$\omega_k = \omega P_k^+ \quad (16)$$
$$N_k = N P_k^- \quad (17)$$

References

1. Khan, I., W. Rehman, W., Rahim, F., Hussain, R., Khan, S., Rasheed, L., Alanazi, A.S., Hefnawy, M., Alanazi, M. M., Shah, S. A. A., Taha, M. (**2023**) Synthesis, in vitro biological analysis and molecular docking studies of new thiadiazole-based thiourea derivatives as dual inhibitors of α-amylase and α-glucosidase. *Arabian Journal of Chemistry,* 16 (9), 105078.
2. Khaldan, A., Bouamrane, S., El-mernissi, R., Ouabane, M., Alaqarbeh, M., Maghat, H., Ajana, M. A., Sekkat, C., Bouachrine, M., Lakhlifi, T., Sbai, A. (**2024**) Design of new α-glucosidase inhibitors through a combination of 3D-QSAR, ADMET screening, molecular docking, molecular dynamics simulations and quantum studies. *Arabian Journal of Chemistry*, 17(3) 105656
3. Mohamed Farhan, H., Nassar, M., Hassan Ahmed, M., Abougabal, K. Abd Elazim Taha, N. (**2022**) An association between the sarcolemmal membrane-associated protein gene and microvascular endothelial diabetic retinopathy in patients with type 2 diabetes mellitus: A preliminary case control study, *Diabetes Metabolic Syndrome*. 16(11), 102653.
4. Taha, M., Rahim, F., Zaman, K., Selvaraj, M., Uddin, N., Farooq, R.K., Nawaz, M., Sajid, M., Nawaz, F., Ibrahim, M., Khan, K.M. (**2019**) Synthesis, α-glycosidase inhibitory potential and molecular docking study of benzimidazole derivatives. *Bioorganic Chemistry.* 95**,** 103555.
5. Whiting, D.R., Guariguata, L., Weil, C., Shaw, J. (**2011**) IDF diabetes atlas: global estimates of the prevalence of diabetes for 2011 and 2030. *Diabetes Research and Clinical Practice.* 94(3), 311–321.
6. Tang, P.C., Lin, Z. G., Wang, Y. (**2010**) Design and synthesis of DPP-4 inhibitor for the treatment of type 2 diabetes. *Chinese Chemical Letters.* 21, 253–256.
7. Taha, M., Alshamrani, F.J., Rahim, F., Hayat, S., Ullah, H., Zaman, K., Imran, S., Khan, K.M., Naz, F. (**2019**) Synthesis of Novel Triazinoindole-Based Thiourea Hybrid: A Study on α-Glucosidase Inhibitors and Their Molecular Docking. *Molecules.* 24(21), 3819.
8. Khaldan, A., Bouamrane, S., El-Mernissi, R., Maghat, H., Ajana, M. A., Sbai, A., Bouachrine, M., Lakhlifi, T. (**2022**) In silico design of new α-glucosidase inhibitors through 3D-QSAR study, molecular docking modeling and ADMET analysis. *Moroccan Journal of Chemistry*. 10(1), 22-36.
9. Yeye, E. O., Kanwal, Mohammed Khan, K., Chigurupati, S., Wadood, A., Ur Rehman, A., Perveen, S., Kannan Maharajan, M., Shamim, S., Hameed, S., Aboaba, S.A., Taha, M. (**2020**) Syntheses, in vitro α-amylase and α-glucosidase dual inhibitory activities of 4-amino-1,2,4-triazole derivatives their molecular docking and kinetic studies*. Bioorganic and Medicinal Chemistry*. 28, 115467.
10. Taha, M., Rahim, F., Zaman, K., Selvaraj, M., Uddin, N., Farooq, R.K., Nawaz, M., Sajid, M., Nawaz, F., Ibrahim, M., Khan, K.M. (**2019**) Synthesis, α-glycosidase inhibitory potential and molecular docking study of benzimidazole derivatives. *Bioorganic Chemistry.* 95, 103555.
11. Lefebvre, P., Scheen, A. (**1994**) The use of acarbose in the prevention and treatment of hypoglycaemia. *European Journal of Clinical Investigation.* 3, 40–44.
12. Scott, L. J., Spencer, C.M. (2000) Miglitol: a review of its therapeutic potential in type 2 diabetes mellitus. *Drugs,* 59(3): 521–549.
13. Dong Y., Sui, L., Yang, F., Ren, X., Xing, Y., Xiu, Z. (**2022**) Reducing the intestinal side effects of acarbose by baicalein through the regulation of gut microbiota: An in vitro study. *Food Chemistry*, 394, 133561.
14. Chavda, V., Patel, S. (**2022**) Voglibose and saxagliptin ameliorate the post-surgical stress and cognitive dysfunction in chronic anaesthesia exposed diabetic MCAo induced ischemic rats. *IBRO Neuroscience Reports.* 13, 426-435.
15. Noori, M., Rastak, M., Halimi, M., Ghomi, M. K., Mollazadeh, M., Mohammadi-Khanaposhtani, M., Sayahi, M. H., Rezaei, Z., Mojtabavi, S., Ali Faramarzi, M., Larijani, B., Biglar, M., Amanlou, M., Mahdavi, M. (**2022**) Design, synthesis, in vitro, and in silico enzymatic evaluations of thieno[2,3-b]quinoline-hydrazones as novel inhibitors for α-glucosidase. *Bioorganic Chemistry*. 127, 105996.
16. Khaldan, A., Bouamrane, S., El-mernissi, R., El Mchichi, L., Maghat, H., Bouachrine, M., Lakhlifi, T., Sbai, A. (**2022**). In search of new potent α-glucosidase inhibitors: molecular docking and ADMET prediction. *Moroccan Journal of Chemistry.* 10 (4), 772-786.
17. Foley, M., Tilley, L. (**1998**) Quinoline antimalarials: mechanisms of action and resistance and prospects for new agents. *Pharmacology Therapeutics.* 79 (1), 55-87.
18. Chen, Y., Hsien-Ming, H., Lu, C., Li, K., Tzeng, C. (**2004**) Synthesis and anticancer evaluation of certain indolo[2,3-b]quinoline derivatives. *Bioorganic Medicinal Chemistry.* 12(24), 6539-6546.
19. Bekhit, A. A., El-Sayed, O. A., Aboulmagd, E., Park, J. Y. (**2004**) Tetrazolo[1,5-a]quinoline as a potential promising new scaffold for the synthesis of novel anti-inflammatory and antibacterial agents. *European Journal of Medicinal Chemistry.* 39 (3), 249-255.
20. Taha, M., Ismail, N. H., Imran, S., Wadood, A., Fazal Rahim, F., Ali, M., Ur Rehman, A. (**2015**) Novel Quinoline Derivatives as Potent In Vitro α-Glucosidase Inhibitors: In Silico Studies and SAR Predictions. *MedChemComm,* **6**(10), 1826-1836.

21. Khaldan, A., Bouamrane, S., El-mernissi, R., Maghat, H., Ajana, M. A., Sbai, A., Bouachrine, M., Lakhlifi, T. (**2021**) Identification of potential α-glucosidase inhibitors: 3D-QSAR modeling, molecular docking approach. *Rhazes: Green and applied chemistry.* 12, 60-75
22. Khaldan, A., Bouamrane, S., El-mernissi, R., Maghat, H., Ajana, M.A., Sbai, A., Bouachrine, M. Lakhlifi, T. (**2021**) 3D-QSAR modeling, molecular docking and ADMET properties of benzothiazole derivatives as a-glucosidase inhibitors. *Material Today: Preceding.* 45(8), 7643- 7652.
23. Vilar, S., Cozza, G. & Moro, S. (**2008**) Medicinal chemistry and the molecular operating environment (MOE): application of QSAR and molecular docking to drug discovery. *Current Topics in Medicinal Chemistry,* 8(18), 1555–1572.
24. Khaldan, A., El khatabi, K., El-mernissi, R., Sbai, A., Bouachrine, M., Lakhlifi, T. (**2020**) Combined 3D-QSAR Modeling and Molecular Docking Study on metronidazole-triazole-styryl hybrids as antiamoebic activity. *Moroccan Journal of Chemistry*. 8(1), 527-539.
25. El Khatabi, K., Aanouz, I., EL-Mernissi, R., Khaldan, A., Ajana, M.A., Bouachrine, M., Lakhlifi, T. (2020) Design of Novel Benzimidazole Derivatives as Potential α-amylase Inhibitors by 3D-QSAR Modeling and Molecular Docking Studies. *Journal of the Turkish Chemical Society Section A: Chemistry*. 7(2): 471-480.
26. Khaldan, A., Bouamrane, S., El-mernissi, R., Maghat, H., Ajana, M.A., Sbai, A., Bouachrine, M., Lakhlifi, T. (**2022**) In silico study of 2,4,5-trisubstituted thiazoles as inhibitors of tuberculosis using 3D-QSAR, molecular docking, and ADMET analysis. *El-Cezerî Journal of Science and Engineering.* 9(2), 452-468.
27. EL-Mernissi, R., El Khatabi, K., Khaldan, A., El Mchichi, L., Ajana, M.A., Bouachrine, M., Lakhlifi, T. (**2021**) Design of new 3, 5-disubstituted indole as hematological anticancer agents using 3D-QSAR, molecular docking and drug-likeness studies. *Materials Today: Proceedings.* 45, 7608–7614.
28. Bouamrane, S., Khaldan, A., Hajji, H., El-mernissi, R., Maghat, H., Ajana, M.A., Sbai, A., Bouachrine, M., Lakhlifi, T. (**2022**) 3D-QSAR, molecular docking, molecular dynamic simulation, and ADMET study of bioactive compounds against candida albicans. *Moroccan Journal of Chemistry*. 10(3), 523-541.
29. Ouabane, M., Tabti, K., Hajji, H., Elbouhi, M., Khaldan, A., Elkamel, K., Sbai, A., Ajana, M.A., Sekkat, C., Bouachrine, M., Lakhlifi, T. (**2023**) Structure-odor relationship in pyrazines and derivatives: A physicochemical study using 3D-QSPR, HQSPR, Monte Carlo, molecular docking, ADME-Tox and molecular dynamics. *Arabian Journal of Chemistry*. 2023, 16, 105207.
30. Khaldan, A., Agorram, A., Ghaleb, A. Aouidate, A. Sbai, A., M. Bouachrine, M., Lakhlifi, T. (**2019**) 3D QSAR Modeling and Molecular Docking Studies on a series of quinolone-triazole derivatives as antibacterial agents. *Rhazes: Green and Applied Chemistry*. 6, 11-26.
31. Klebe, G., Abraham, U. & Mietzner, T. 1994. Molecular similarity indices in a comparative analysis (CoMSIA) of drug molecules to correlate and predict their biological activity. *Journal of Medicinal Chemistry,* 37(24): 4130–4146.
32. Khaldan, A., Bouamrane, S., El-Mernissi, R., El Khatabi, K., Aanouz, I., Aggoram, A., Sbai, A., Bouachrine, M., Lakhlifi, T. (**2021**) QSAR study of α-Glucosidase inhibitors for benzimidazole bearing bis-Schiff bases using CoMFA, CoMSIA, and molecular docking. *International Journal of Quantitative Structure-Property Relationships.* 6(1), 9–24.
33. Khaldan, A., Bouamrane, S., El-mernissi, R., Maghat, H., Sbai, A., M. Bouachrine, M., Lakhlifi, T. (**2023**) Molecular docking, ADMET prediction and quantum computational on 2-methoxy benzoyl hydrazone compounds as potential antileishmanial inhibitors. *Biointerface Research in Applied Chemistry*. 4, 302.
34. El-Mernissi, R., Khaldan, A., ElMchichi, L., Ajana, M.A., Lakhlifi, T., Bouachrine, M. (**2022**) 3D-QSAR, ADMET, and molecular docking studies for designing new 1, 3, 5-triazine derivatives as anticancer agents. *Egyptian Journal of Chemistry*. 65(132), 9-18.
35. Pires, D.E.V., Blundell, T.L., Ascher, D.B. (**2015**) pkCSM: Predicting small-molecule pharmacokinetic and toxicity properties using graph-based signatures. *Journal of Medicinal Chemistry. 58(9),* 4066–4072.
36. Daina, A., Michielin, O., Zoete, V. (**2017**). SwissADME: A free web tool to evaluate pharmacokinetics, drug-likeness and medicinal chemistry friendliness of small molecules. *Scientific Reports*. **7**, 42717.
37. EL-Mernissi, R., El Khatabi, K., Khaldan, A., Bouamrane, S., El Mchichi, L., Ajana, M.A., Bouachrine, M., Lakhlifi T. (**2021**) 3D-QSAR, ADMET and Docking Studies for design new 5,5-Diphenylimidazolidine-2,4-dione derivatives agents against cervical cancer. *Orbital: Electron Journal of Chemistry*. 14(1), 24-32.
38. Veber, D.F., Johnson, S.R., Cheng, H.Y., Smith, B.R., Ward, K.W., Kopple, K.D. (**2002**) Molecular properties that influence the oral bioavailability of drug candidates. *Journal of Medicinal Chemistry*. 45(12), 2615-2623.
39. Khaldan, A., Bouamrane, S., El-mernissi, R., Alaqarbeh, M., Alsakhen, N., Maghat, H., Ajana, M.A., Sbai, A., Bouachrine, M., Lakhlifi, T. (2022) Computational study of quinoline-based thiadiazole compounds as potential antileishmanial inhibitors. *New Journal of Chemistry*. 46, 17554.
40. Khaldan, A., Bouamrane, S., En-Nahli, F., El-Mernissi, R., El Khatabi, K., Hmamouchi, R., Maghat, H., Ajana, M. A, Sbai, A., Bouachrine, M., Lakhlifi, T. (**2021**) Prediction of potential inhibitors of SARS-CoV-2 using 3D-QSAR, molecular docking modeling and ADMET properties. Heliyon, 7, e06603.
41. Sultana, S., Hossain, Md. A., Islam, Md. M., Kawsar, S. M. A. (2024) Antifungal potential of mannopyranoside derivatives through computational and molecular docking studies against Candida albicans 1IYL and 1AI9 proteins. *Current Chemistry Letters.* 13(1), 1-14.

42. Anees Pangal, Pranav Tambe, Khursheed Ahmed. (2023) Screening of 3-acetylcoumarin derivatives as multifunctional biological agents. *Current Chemistry Letters.* 12(2), 343-352
43. Šrejber, M., Navrátilová, V., Paloncýová, M., Bazgier, V., Berka, K., Anzenbacher, P. & Otyepka, M. 2018. Membrane-attached mammalian cytochromes P450: an overview of the membrane's effects on structure, drug binding, and interactions with redox partners. *J. Inorg. Biochem.* **183**: 117–136.
44. EL-Mernissi, R., Khaldan, A., Bouamrane, S., Rehman, H.M., Alaqarbeh, M. Ajana, M.A. Lakhlifi, T., Bouachrine, M. (2024) 3D-QSAR, molecular docking, simulation dynamic and ADMET studies on new quinolines derivatives against colorectal carcinoma activity, *Biomolecular Structure and Dynamics*. 42(7), 3682-3699.
45. Ortiz, C.L.D., Completo, G. C., Nacario, R. C., Nellas, R. B. (**2019**) Potential Inhibitors of Galactofuranosyltransferase 2 (GlfT2): Molecular Docking, 3D-QSAR, and In Silico ADMETox Studies. *Scientific Report.* 9, 17096.
46. Kramer, B., Rarey, M., Lengauer, T. (**1999**) Evaluation of the FLEXX incremental construction algorithm for protein-ligand docking. *Proteins*, 37(2), 228–241.
47. Al-horaibi, S. A., Alghamdi, M.T., Gaikwad, S.T., Rajbhoj, A. S. (**2018**) Comparison and Determine Characteristics Potentials of HOMO/ LUMO and Relationship between Ea and Ip for Squaraine Dyes (SQ1, SQ2) by Using Cyclic Voltammetry and DFT/TD-DFT, *Moroccan Journal of Chemistry*. 6(3), 404-4013.
48. Jaramillo, P., Domingo, L.R., Chamorro, E., Pérez, P., (**2008**) A further exploration of a nucleophilicity index based on the gas-phase ionization potentials. *Journal of Molecular Structure: Theochem*, 865(1-3), 68–72.
49. Domingo, L.R.; Aurell, M.J.; Pérez, P.; Contreras, R. (**2002**) Quantitative characterization of the local electrophilicity of organic molecules. Understanding the regioselectivity on Diels-Alder reactions. *J. Phys. Chem. A* 106, 6871–6875.
50. Azaid, A., Abram, T., Alaqarbeh, M., Raftani, M., Kacimi, R., Sbai, A., Lakhlifi, T., Bouachrine, M. (2023) Design new organic material based on triphenylamine (TPA) with D-π-A-π-D structure used as an electron donor for organic solar cells: A DFT approach, *Journal of Molecular Graphics and Modelling*, 122, 108470..
51. Taha, M., Sultan, S., Imran, S., Rahim, F., Zaman, K., Wadood , A., Ur Rehman, A., Uddin, N. Khan, K.M. (**2019**) Synthesis of quinoline derivatives as diabetic II inhibitors and molecular docking studies. *Bioorganic Medicinal Chemistry.* 27(18), 1081-4088.
52. Sybyl 8.1; Tripos Inc.: St. Louis, MO, USA, 2008; Available online: http://www.tripos.com (accessed on 26 January 2011).
53. Clark, M., Cramer, R.D. & Van Opdenbosch, N. 1989. Validation of the general purpose tripos 5.2 force field. *Journal* of *Computational Chemistry.* 10, 982–1012.
54. Sainy, J., Sharma, R. (**2015**) QSAR analysis of thiolactone derivatives using HQSAR, CoMFA and CoMSIA. SAR. QSAR. *Environmental Research*. 26, 873-892.
55. Waller, C.L. (2004) A Comparative QSAR Study Using CoMFA, HQSAR, and FRED/SKEYS Paradigms for Estrogen Receptor Binding Affinities of Structurally Diverse Compounds. *Journal of chemical information and computer sciences*. 44, 758-765.
56. Jiao, L., Zhang, X., Qin, Y., Wang, X., Li, H. (**2016**) Hologram QSAR study on the electrophoretic mobility of aromatic acids. *Chemometrics and Intelligent Laboratory Systems*. 157, 202-207.
57. Wold, S. (**1991**). Validation of QSAR's. *Quantitative Structure Activity Relationships*, 10(3), 191–193.
58. Golbraikh, A., Tropsha, A. (**2002**) Beware of q2!. Journal of Molecular Graphics and Modelling, 20, 269–276.
59. Roy, K., (**2007**) On some aspects of validation of predictive quantitative structure–activity relationship models. Expert Opinion on Drug Discovery, 2, 1567–1577.
60. Bouamrane, S., Khaldan, A., Hajji, H., El-mernissi, R., Alaqarbeh, M., Alsakhen, N., Maghat, H., Ajana, M.A., Sbai, A., Bouachrine, M., Lakhlif, T. (**2023**) In silico identification of 1,2,4-triazoles as potential Candida Albicans inhibitors using 3D-QSAR, molecular docking, molecular dynamics simulations, and ADMET profiling. *Molecular Diversity*. 27(5), 2111-2132
61. Bouamrane, S., Khaldan, A., Alaqarbeh, M., Sbai, A., Ajana, M.A., Lakhlifi, T., Bouachrine, M. (2024) Computational integration for antifungal 1,2,4-triazole inhibitors design: QSAR, molecular docking, molecular dynamics simulations, ADME/Tox, and retrosynthesis studies. *Chemical Physics Impact*. 8,100502.
62. Rahim, F., Ullah, H., Javid, M. T., Wadood, A., Taha, M., Ashraf, M., Shaukat, A., Junaid, M., Hussain, S., Rehman, W., Mehmood, R., Sajid, M., Khan, M. N., Khan, K.M., 2015. Synthesis, in vitro evaluation and molecular docking studies of thiazole derivatives as new inhibitors of α-glucosidase. Bioorganic Chemistry, 62, 15-21.
63. Trott, O., Olson, A.J. (**2010**) AutoDock Vina: improving the speed and accuracy of docking with a new scoring function, efficient optimization, and multithreading. *Journal of Computational Chemistry*. 3(2), 455–461.
64. Hamaamin Hussen, N., Hameed Hasan, A., Jamalis J., Shakya, S., Chander, S., Kharkwal, H., Murugesan, S., Ajit Bastikar, V., Pyarelal Gupta, P. (2022) Potential inhibitory activity of phytoconstituents against black fungus: In silico ADMET, molecular docking and MD simulation studies. *Comput Toxicol*, 24, 100247.
65. Dassault Systèmes BIOVIA. (**2016**). Discovery studio modeling environment, release 2017, San Diego: Dassault Systèmes. [WWW document], 2016. http://accelrys.com/products/collaborativescience/biovia-discovery-studio/. Accessed 25 Feb 17.

66. DeLano,W. (**2002**). The PyMOL Molecular Graphics System DeLano Scientific, Palo Alto, CA, USA, 2002. http://www.pymol.org. (Accessed 25 February 2017).
67. Jo, S., Kim, T., Iyer, V.G., Im, W. (2008) CHARMM-GUI: a web-based graphical user interface for CHARMM. *Journal of Computational Chemistry*, 29(11), 1859-1865.
68. Lee, J., Cheng, X., Swails, J.M., Yeom, M.S., Eastman, P.K., Lemkul, J.A, Wei, S., Buckner, J., Jeong, J. C., Qi, Y., Jo, S., Pande, V.S., Case, D.A., Brooks 3rd, C.L., MacKerell Jr, A.D., Klauda, J.B., Im, W., 2016. CHARMM-GUI Input Generator for NAMD, GROMACS, AMBER, OpenMM, and CHARMM/OpenMM Simulations Using the CHARMM36 Additive Force Field. *Journal of Chemical Theory and Computation*. 12(1), 405-413.
69. Best, R.B., Zhu, X., Shim, J., Lopes, P.E., Mittal, J., Feig, M., Mackerell Jr, A.D. (**2012**) Optimization of the additive CHARMM all-atom protein force field targeting improved sampling of the backbone φ, ψ and side-chain χ(1) and χ(2) dihedral angles . *Journal of Chemical Theory and Computation.* 8(9), 3257-3273.
70. Yu, W., He, X., Vanommeslaeghe, K., MacKerell Jr, A.D., (**2012**) Extension of the CHARMM General Force Field to sulfonyl-containing compounds and its utility in biomolecular simulations. *Journal of Computational Chemistry*. 33(31), 2451-68.
71. Jorgensen, W.L., Chandrasekhar, J., Madura, J.D. (**1983**) Comparison of simple potential functions for simulating liquid water. *The Journal of Chemical Physics*. 79, 926-935.
72. Darden, T., York, D., Pedersen, L. (**1993**) Particle mesh Ewald: An N·log(N) method for Ewald sums in large systems. *The Journal of Chemical Physics*, 98, 10089-10092.
73. Frisch, M. (**2009**) GAUSSIAN 09. Revision E. 01, Gaussian Inc.
74. Koopmans, T., (**1934**) Über die Zuordnung von Wellenfunktionen und Eigenwerten zu deninzelnen Elektronen Eines atoms, *Physica*, 1, 104–113
75. Domingo, L. R., Perez, P., Saez, J. A. (**2013**). Understanding the local reactivity in polar organic reactions through electrophilic and nucleophilic Parr functions. RSC Advances., 3(5), 1486–1494.